

Phase change thermal interface materials: From principles to applications and beyond

Chenggong Zhao(赵成功), Yifan Li(李一凡), Chen Jiang(蒋晨), Yuanzheng Tang(唐元政), Yan He(何燕), Wei Yu(于伟), and Bingyang Cao(曹炳阳)

Citatio: Chin. Phys. B, 2025, 34 (**9**): 096301. DOI: 10.1088/1674-1056/ade59f
http://cpb.iphy.ac.cn; http://iopscience.iop.org/cpb

What follows is a list of articles you may be interested in

Normal energy and stretch diffusion in a one-dimensional momentum conserving lattice with nonlinear bounded kinetic energy

Hongbin Chen(陈宏斌), Qin-Yi Zhang(张钦奕), Jiahui Wang(王佳惠), Nianbei Li(李念北), and Jie Chen(陈杰)
Chin. Phys. B, 2025, 34 (**9**): 094401. DOI: 10.1088/1674-1056/addce5

Dynamic response of a thermal transistor to time-varying signals

Qinli Ruan(阮琴丽), Wenjun Liu(刘文君), and Lei Wang(王雷)
Chin. Phys. B, 2024, 33 (**5**): 056301. DOI: 10.1088/1674-1056/ad2dcc

General three-dimensional thermal illusion metamaterials

Tianfeng Liu(刘天丰), Zhaochen Wang(王兆宸), Zhan Zhu(朱展), and Run Hu(胡润)
Chin. Phys. B, 2024, 33 (**4**): 044401. DOI: 10.1088/1674-1056/ad09aa

Impeded thermal transport in aperiodic BN/C nanotube superlattices due to phonon Anderson localization

Luyi Sun(孙路易), Fangyuan Zhai(翟方园), Zengqiang Cao(曹增强), Xiaoyu Huang(黄晓宇), Chunsheng Guo(郭春生), Hongyan Wang(王红艳), and Yuxiang Ni(倪宇翔)
Chin. Phys. B, 2023, 32 (**5**): 056301. DOI: 10.1088/1674-1056/acb9e7

Lattice thermal conduction in cadmium arsenide

R F Chinnappagoudra, M D Kamatagi, N R Patil, and N S Sankeshwar
Chin. Phys. B, 2022, 31 (**11**): 116301. DOI: 10.1088/1674-1056/ac7863

TOPICAL REVIEW — Heat conduction and its related interdisciplinary areas

Phase change thermal interface materials: From principles to applications and beyond

Chenggong Zhao(赵成功)[1,2], Yifan Li(李一凡)[2,3,†], Chen Jiang(蒋晨)[2], Yuanzheng Tang(唐元政)[1], Yan He(何燕)[1], Wei Yu(于伟)[1,2], and Bingyang Cao(曹炳阳)[1,3,‡]

[1] *School of Electromechanical Engineering, Qingdao University of Science and Technology, Qingdao* 266061, *China*
[2] *School of Energy and Materials, Shanghai Polytechnic University, Shanghai* 201209, *China*
[3] *Key Laboratory for Thermal Science and Power Engineering of Ministry of Education, Department of Engineering Mechanics, Tsinghua University, Beijing* 100084, *China*

(Received 7 April 2025; revised manuscript received 28 May 2025; accepted manuscript online 18 June 2025)

Phase change thermal interface materials (PC-TIMs) have emerged as a promising solution to address the increasing thermal management challenges in electronic devices. This is attributed to their dual mechanisms of latent heat absorption and phase change-induced interfacial wettability. This review explores the fundamental principles, material innovations, and diverse applications of PC-TIMs. The heat transfer enhancement mechanisms are first underlined with key factors such as thermal carrier mismatch at the microscale and contact geometry at the macroscale, emphasizing the importance of material selection and design for optimizing thermal performance. Section 2 focuses on corresponding experimental approaches provided, including intrinsic thermal conductivity improvements and interfacial heat transfer optimization. Section 3 discusses common methods such as physical adsorption via porous materials, chain-crosslinked network designs, and core–shell structures, and their effects on leakage prevention, heat transfer enhancement, and application flexibility. Furthermore, the extended applications of PC-TIMs in thermal energy storage are explored in Section 4, suggesting their potential in diverse technological fields. The current challenges in interfacial heat transfer research and the prospect of PC-TIMs are also discussed. The data-driven machine learning technologies will play an increasingly important role in addressing material development and performance prediction.

Keywords: phase change thermal interface materials, contact thermal resistance, interfacial heat transfer, encapsulation

PACS: 63.20.k–, 44.10.+i, 81.05.–t

DOI: 10.1088/1674-1056/ade59f **CSTR:** 32038.14.CPB.ade59f

1. Introduction

The rapid development of new-generation information and communication technologies, such as 5G, AI, and cloud computing, has led to a significant increase in computational demands and heat flux density.[1,2] The introduction of 3D integrated circuit (IC) technology, particularly with the 3 nm process, has further increased packaging density, pushing chip-level heat flux densities to over 1 kW/cm^2.[3,4] Over 50% of microelectronic device failures are caused by thermal management issues, making the development of efficient thermal management materials a critical need for the advancement of electronic systems.[5]

Thermal interface materials (TIMs), which fill the gaps between solid interfaces, are essential for addressing thermal management challenges in electronic devices. In IC packaging, TIMs are typically categorized into two types: TIM1, used between the chip and the lid, and TIM2, positioned between the lid and the heat sink. Conventional TIMs are generally classified into metal-based and polymer-based materials.[6] Metal-based TIMs are typically applied in high heat flux environments without insulation requirements, while polymer-based TIMs are used in less demanding heat dissipation applications where electrical insulation is necessary.[7] Due to the inherently high-power density of chips, TIM1 materials are predominantly electrically insulating, with research focusing on achieving ultra-high thermal conductivity and low coefficient of thermal expansion (CTE) compatible with silicon semiconductors (2.6–3.0$\times10^{-6}$ K^{-1}). In contrast, TIM2 materials are often metal-based, aimed at efficiently transferring heat to heat sinks or external cooling systems. Current research in TIM2 focuses on improving thermal conductivity ($>$ 20 W/(m·K)) and minimizing thermal resistance at the interface ($<$ 0.01 K·cm^2/W).[8] In addition to traditional TIMs, phase change-induced TIMs (PC-TIMs) have emerged as a rapidly developing research area in recent years.[9] During the phase change process, these materials exchange a significant amount of heat with their surroundings while maintaining a nearly constant temperature, allowing for high-capacity ther-

†Corresponding author. E-mail: liyf@sspu.edu.cn
‡Corresponding author. E-mail: caoby@tsinghua.edu.cn

© 2025 Chinese Physical Society and IOP Publishing Ltd. All rights, including for text and data mining, AI training, and similar technologies, are reserved.

mal energy storage. This characteristic enables PC-TIMs to offer high energy density accompanied by low exergy loss during heat transfer. Moreover, as the material transitions from solid to liquid, it can more effectively fill microscopic surface irregularities between electronic components and heat dissipation devices, further reducing thermal resistance.[10,11] The solid–liquid adaptive nature of PC-TIMs allows them to efficiently perform under varying operational conditions, making them suitable for thermal management across a wide range of load demands, from standby to high-performance modes.

It is worth noting that several comprehensive reviews have been published on TIMs and phase change materials (PCMs) in the past decade. Khan *et al.*[12] reviewed the application of carbon-based TIMs in electronic devices. Lewis *et al.*[13] summarized the application of graphene as a thermal filler in TIMs, discussing its potential and prospects. Ma and Feng *et al.*[14,15] discussed the enhancement of thermal conductivity in polymer-based TIMs. Chen *et al.*[16] reviewed recent advancements in liquid metal-based TIMs. Razeeb *et al.*[17] focused more on the practical applications of TIMs, providing an extensive summary of different base systems (carbon-based and metal-based) and filler types. Numerous reviews exist for PCMs, primarily focusing on their applications in thermal energy storage. Liu and Wu *et al.*[18,19] provided summaries and future outlooks on the thermal conductivity enhancement in PCMs. Safari *et al.*[20] explored the supercooling mechanism and applications of PCMs. Lin and Umair *et al.*[21,22] reviewed the developments and challenges of inorganic PCMs and shape-stable organic PCMs, respectively. Shamberger *et al.*[23] summarized the physical properties and melting characteristics of metal-based PCMs. However, there is currently no comprehensive review specifically addressing PCMs for thermal interface applications in electronic devices. It is widely acknowledged that improving thermal conductivity remains a key focus for high-performance PC-TIMs. However, a distinguishing feature of PC-TIMs is their ability to enhance interfacial heat transfer efficiency through improved contact during the phase transition process. Unfortunately, this improvement brings a challenge as there is a potential risk of leakage during this transition. Consequently, research on PC-TIMs is mainly centered around two areas: heat transfer enhancement and packaging improvement, which will also be the primary focus of this review.

This review starts with the mechanisms of TIMs, summarizing the key physical factors affecting heat transfer in their application, such as intrinsic thermal conductivity and interfacial parameters. It also categorizes and summarizes performance enhancement mechanisms reported for PC-TIMs over the past decade. Furthermore, the review discusses the influence of various packaging strategies on both leakage prevention and thermal performance. In addition, the utilization of the heat storage capacity of PCMs is explored as extended applications, although some examples may not directly pertain to the thermal interface field of electronic devices. Efficient use of heat storage in PC-TIMs not only conserves energy but also facilitates long-term stability. The authors hope that this part will inspire researchers to develop heat-utilization materials or devices that can be coupled with PC-TIMs, further advancing their practical application in thermal management in cutting-edge electronic systems. Figure 1 illustrates the specific discussed contents in this review.

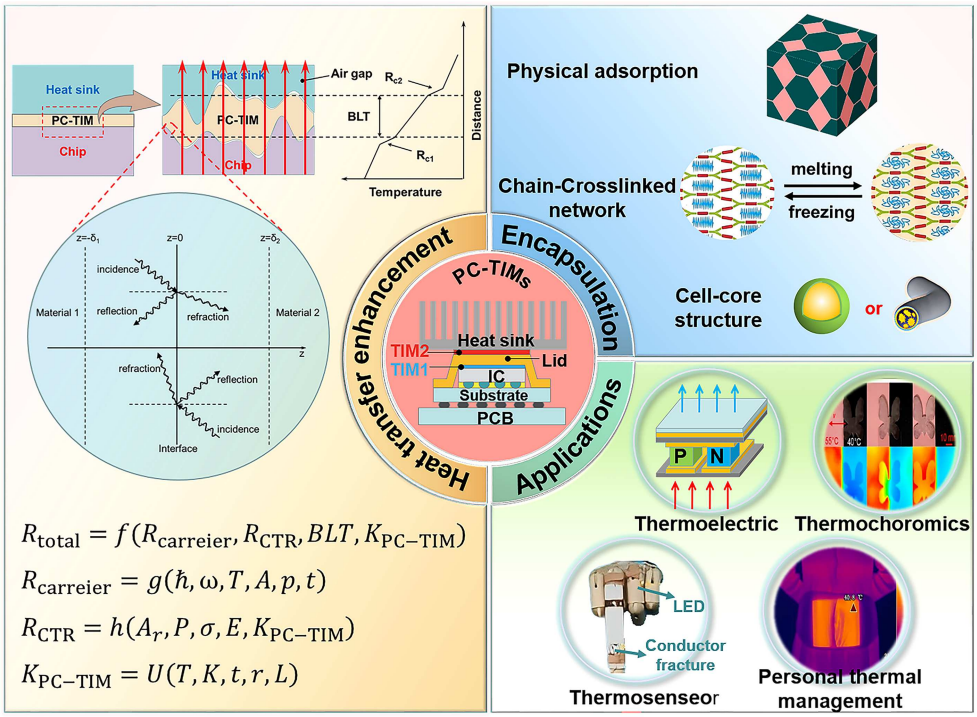


Fig. 1. Schematic diagram of the discussed content in this review.

2. Heat transfer enhancement

2.1. Insights to contact heat transfer in electric devices

The primary heat transfer mode in electronic devices at the contact interface is solid-to-solid conduction, and the inherent material property differences on both sides of the interface lead to heat transfer losses. These losses are typically characterized by contact thermal resistance (CTR). The actual contact surfaces are not perfectly smooth, often containing small air gaps. Due to the extremely low thermal conductivity of air, these gaps significantly increase the CTR. The purpose of filling the interface between the heat source and the heat sink with a TIM is to reduce the total thermal resistance (R_{total}) of the "heat source/TIM/heat sink" path, which is lower than the direct R_{total} between the "heat source/heat sink". Compared to traditional TIMs, PC-TIMs offer superior interface filling, which is primarily due to the phase change of the encapsulated PCMs upon heating, which undergo a solid-to-liquid transition. This phase change imparts flexibility to the material, improving the contact quality at the interface and enhancing heat transfer efficiency.

Similar to most TIMs, the performance of PC-TIM can be evaluated using the R_{total} of the "heat source/PC-TIM/heat sink" interface,[24]

$$R_{\text{total}} = \frac{\Delta T}{q}, \tag{1}$$

where ΔT represents the temperature difference across the interface, and q denotes the heat transferred per unit area per unit time. The physical meaning of R_{total} is the temperature drop induced by the unit heat flux across the interface. To gain deeper insight into the factors influencing R_{total}, the heat source, PC-TIM, and heat sink can be considered as separate entities for studying the factors affecting CTR. In this case, R_{total} follows a series thermal resistance model,[25]

$$R_{\text{total}} = R_{\text{c1}} + R_{\text{TIM}} + R_{\text{c2}}. \tag{2}$$

The bulk thermal resistance of the TIM can be calculated by[25]

$$R_{\text{TIM}} = \frac{BLT}{K_{\text{TIM}}}, \tag{3}$$

where BLT is the bond line thickness (effective thickness) of the TIM, and K_{TIM} is the intrinsic thermal conductivity of the TIM. R_{c1} and R_{c2} represent the CTR between the two mated surfaces (heat source/TIM and heat source/TIM). As shown in Eqs. (2) and (3), when the BLT is fixed, the R_{total} value can be reduced by decreasing CTR and enhancing K_{TIM}. The development and practical application of PC-TIM will be discussed from these two perspectives.

2.2. Influence mechanism of CTR

According to Eq. (2), in addition to the intrinsic thermal conductivity of PC-TIM, the thermal resistances at both contact surfaces (R_{c1} and R_{c2}) are also important components of R_{total}. The thermal resistance can be analyzed at two scales: the microscopic interfacial resistance (Kapitza resistance) and the macroscopic contact resistance.[15,26] The former refers to the thermal resistance at an ideal interface, specifically at the solid–solid contact or the solid–liquid interface resulting from slight liquefaction of the PC-TIM surface, where thermal carrier mismatch induces thermal resistance. The latter arises from geometric structural factors, specifically the thermal resistance due to insufficient heat transfer caused by surface parameters such as roughness. It is generally considered that the former is one to two orders of magnitude smaller than the latter.[27,28] For the practical application scenario of TIMs, the adjacent surfaces are often composed of semiconductor or metallic materials (heat sinks). The thermal carrier mismatch becomes particularly significant when employing polymer-based TIMs.[29–31] The actual contact area is influenced by interfacial factors such as surface roughness and contact pressure.[32,33] A comprehensive evaluation of the key factors influencing interfacial heat transfer is crucial for expanding the practical applications of PC-TIMs.

2.2.1. Mismatch of thermal carriers

The coupling of thermal carriers across an interface typically occurs between electrons in metals and phonons in non-metals, as shown in Fig. 2(a).[34–37] Current research on phonon scattering at interfaces primarily focuses on computational modeling and simulations, with the main goal of improving the coupling and matching efficiency of thermal carriers at these interfaces.[38–41] Typical methods for calculating the ideal interface (Kapitza thermal resistance) include the Newtonian mechanics-based lattice dynamics (LD) and molecular dynamics (MD), the Green's function (GF) describing the system's response to perturbations, and the Boltzmann transport equation (BTE) describing the particle distribution function.[27] Table 1 summarizes the expressions of those approaches with specific characteristics provided.

Approaches to addressing thermal carrier mismatch between different materials primarily involve interface modification, including self-assembled monolayers (SAMs), plasma treatment, and chemical etching, among which SAMs are the most employed strategy. Self-supported monolayers enable carrier-matching transitions via amphiphilic functional groups, which promote the alignment of carrier transport characteristics across the interface. Lu *et al.*[29] introduced highly oriented SAMs at the polystyrene (PS)/Si interface and discovered that SAMs with short chains and high density more effectively enhance interfacial thermal conductivity

through molecular dynamics simulation (Fig. 2(b)). The Si–O covalent bonds at the Si/SAM interface create a similar chemical structure to that of the PS/SAM interface. Compared to the weaker van der Waals interactions at the Si/PS interface, this structure significantly improves phonon matching at the interface. Experimental results demonstrated a maximum interfacial thermal conductance of 11±1 MW/(m^2·K) for PS/Si and 56±17 MW/(m^2·K) for PS/SAM/Si. Careful selection of functional groups is crucial, as their interfacial performance can vary markedly with the specific substrate or interface configuration. He *et al.*[47] further investigated how SAMs with different terminal groups (–Cl, –CH_3, –SH, and –NH_2) influence interfacial thermal conductance (Fig. 2(c)). They found that introducing –Cl resulted in the largest increase in interfacial thermal conductance, from 52.18 MW/(m^2·K) to 316.73 MW/(m^2·K). This is due to the strong non-bonded interactions and high compatibility between –Cl-SAM and PS, as evidenced by the highest overlap in vibrational spectra.

Table 1. Calculation approaches for Kapitza thermal resistance (R).[42–46]

Type	Model	Characteristic
LD[42]	$R=\frac{1}{\int_0^\infty \hbar\omega\Gamma_{\mathrm{LD}}(\omega)\frac{\partial\bar{n}(\omega,T)}{\partial T}\,\mathrm{d}\omega}$,	the exact lattice structure required
MD	NEMD:[43] $R=\frac{\Delta T}{J}$, $J=\frac{1}{2tA}\sum_{\text{transfer}}\frac{m}{2}(v_{\text{hot}}^2-v_{\text{cold}}^2)$,	proper potential function required
	EMD (infinitely large system):[44] $R=\frac{k_{\mathrm{B}}T^2}{A\int_0^\infty\langle J(t)J(0)\rangle\,\mathrm{d}t}$,	
	EMD (finite system):[44] $R=\frac{\mathrm{e}^{-wt_{\mathrm{s}}}k_{\mathrm{B}}T^2}{A\int_0^{t_{\mathrm{s}}}\langle J(t)J(0)\rangle\,\mathrm{d}t}$,	
GF[45]	$R=\frac{2\pi A}{\int_0^\infty\hbar\omega\frac{\partial\bar{n}(\omega,T)}{\partial T}\Xi(\omega)\,\mathrm{d}\omega}$,	exact lattice structure and force constants required
BTE[46]	$R=\frac{4}{\int_0^{\omega_{\max}}\hbar\omega\sum_p(v(\omega,p)D(\omega,p))\frac{\partial\bar{n}(\omega)}{\partial T}\Xi(\omega)\,\mathrm{d}\omega}$,	empirical boundary condition

LD: $\hbar$ is the reduced Planck constant; ω is the phonon frequency; $\Gamma_{\mathrm{LD}}(\omega)$ is the frequency-dependent transmission spectral density; $\bar{n}(\omega,T)$ is the distribution function of phonons incident on the interface as the following equilibrium one given by the Bose–Einstein distribution, and T is temperature.
MD: ΔT is the temperature difference; J is the heat flux; A is the interfacial cross-section area; k_{B} is the Boltzmann constant; v_{hot} and v_{cold} stand for the velocities of atoms with mass m in the "hot" and "cold" layers; w is a constant and t_{s} is the integration time.
GF: A is the interfacial cross-section area; $\hbar$ is the reduced Planck constant; ω is the phonon frequency; $\bar{n}(\omega,T)$ is the distribution function of phonons incident on the interface as the following equilibrium one given by the Bose–Einstein distribution. The energy-dependent transmission function $\Xi(\omega)$ is the energy-dependent transmission function across the interface.
BTE: $\hbar$ is the reduced Planck constant; $v(\omega,p)$ and $D(\omega,p)$ are the phonon group velocity and the density of states, respectively, at frequency ω and polarization p. $\bar{n}(\omega)$ is the distribution function of phonons; T is the temperature; $\Xi(\omega)$ is the energy-dependent transmission function across the interface.

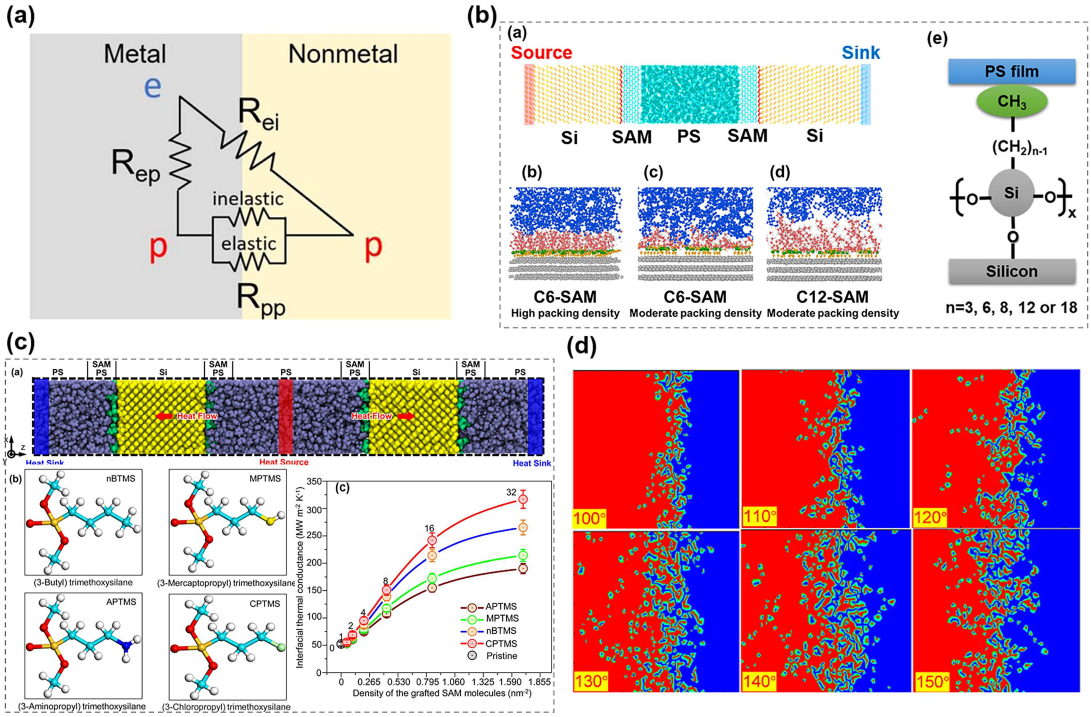


Fig. 2. (a) Diagram of thermal carrier change at the interface of metal and non-metal, reproduced with permission from Ref. [34]; (b) comparison between the geometric structure of SAM and packing density by Lu *et al.*, reproduced with permission from Ref. [29]; (c) the influence of SAMs with different terminal groups (–Cl, –CH_3, –SH, and –NH_2) on interfacial thermal conductance by He *et al.*, reproduced with permission from Ref. [47]; (d) the effect of equilibrium bond angle in SAMs on the interfacial thermal conductance of molten PEG/Au by Song *et al.*, reproduced with permission from Ref. [48].

Additionally, Song *et al.*[48] investigated the effect of equilibrium bond angle in SAMs on the interfacial thermal conductance of molten PEG/Au. They found that increasing the bond angle from 100° to 150° reduced interfacial thermal resistance from 140.85×10^{-9} m^2·K/W to 113.79×10^{-9} m^2·K/W, primarily due to the increased contact area between the molten PEG and SAM molecules (Fig. 2(d)).

It should be noted that research on the mismatch of thermal carriers at the interface between PC-TIMs and metals is limited. This is primarily because the main sources of thermal resistance at the organic PCMs and metal interface are considered macroscopic factors, such as surface roughness and contact pressure, rather than phonon scattering at the microscopic level. Additionally, the complex molecular structure and amorphous nature of organic PCMs make modeling and simulating their phonon behavior highly challenging. Furthermore, the large difference in thermal expansion coefficients between organic materials and metals often leads to mechanical stress at the interface, which has a more pronounced impact on heat transfer, further impairing the relevance of the studies in this context.

2.2.2. Geometry-induced heat loss

Theoretically, solid heat conduction by mechanical contact is the primary determinant of interfacial heat transfer. Wang *et al.*[2] claimed that point-to-point contact accounts for only 2% of the total contact area, with the remainder filled by air. The irregularity of interfacial geometry causes thermal flux constriction, resulting in higher heat transfer efficiency in areas of close contact and lower efficiency in other regions (Fig. 3(a)).

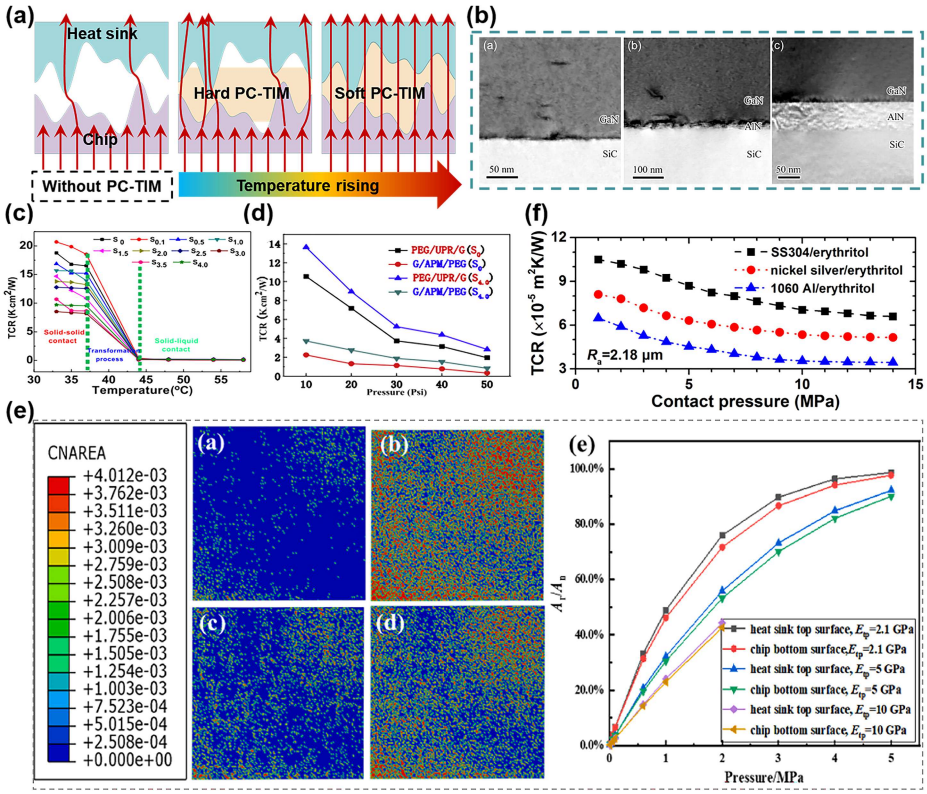


Fig. 3. (a) Mechanism of PC-TIM for interfacial heat transfer enhancement; (b) reduced surface roughness by inserting an AlN layer at the GaN/SiC interface by Li *et al.*, reproduced with permission from Ref. [49]; (c) effect of PC-TIM phase transition on CTR by Liu *et al.*, reproduced with permission from Ref. [50]; (d) the effects of open and closed encapsulation strategies on the CTR of PC-TIMs by Liu *et al.*, reproduced with permission from Ref. [51]; (e) influence of elastic modulus of PC-TIM on contact area by Ren *et al.*, reproduced with permission from Ref. [52]; (f) the relationship between metal hardness and CTR at the metal/erythritol interface by Feng *et al.*, reproduced with permission from Ref. [54].

The influence of surface roughness on macroscopic contact thermal resistance primarily focuses on interfacial modifications. Lu *et al.*[29] demonstrated that introducing SAMs with long alkyl chains increases surface roughness and a higher thermal resistance was observed. This is attributed to the potential bending and deformation of the long chains, leading to more disordered structures. Li *et al.*[49] introduced an AlN layer at the GaN/SiC interface, reducing surface roughness by adjusting lattice mismatch (Fig. 3(b)). This modification resulted in a corresponding decrease in CTR by approximately 0.5 m^2·K/GW. Different from traditional TIMs, PC-TIMs improve interfacial contact by inducing thermally-driven flexibility through phase transition upon heating, thereby reducing thermal resistance. Liu *et al.*[50] proposed that polymer-based PC-TIMs undergo slight surface liquefaction during heating, which subsequently reduces thermal contact resistance. They fabricated the composite PC-TIM composed of olefin block copolymer (OBC), paraffin, and graphene.

They found that as the temperature increased from 37 °C to 45 °C, the CTR sharply decreased from 8–20 cm^2·K/W to 0.1–0.2 cm^2·K/W. This reduction is attributed to the transition from solid–solid contact to solid–liquid contact, enhancing the wettability and effective contact area between the two interfaces (Fig. 3(c)). Furthermore, they investigated the effects of open and closed encapsulation strategies on the CTR of PC-TIMs.[51] As shown in Fig. 3(d), when encapsulating the PCM with acrylic polymer foamed microspheres featuring a microporous structure, the CTR significantly reduced to 0.5–0.9 cm^2·K/W (65 °C, 40 Psi). In contrast, encapsulation using unsaturated polyester resin resulted in a CTR of approximately 3.5–5.3 cm^2·K/W. These findings further demonstrate that increased interfacial wettability resulting from slight surface liquefaction is beneficial for enhancing interfacial heat transfer efficiency.

Another key factor influencing the actual contact area is contact pressure. It is widely recognized that higher pressure can flatten surface roughness, allowing more contact points to come into direct contact.[52,53] Ren *et al.*[52] quantified the actual contact condition between the chip and the TIM using the ratio of actual contact area to nominal contact area. They observed that under a pressure of 5 MPa, the TIM with an elastic modulus of 2.1 GPa achieved twice the contact area compared to the TIM with an elastic modulus of 10 GPa. This increase in contact area is due to the lower elastic modulus, which allows for better surface conformity, as shown in Fig. 3(e). Feng *et al.*[54] investigated the relationship between metal hardness and CTR at the metal/erythritol interface. Their results showed that softer metals undergo greater micro-deformation, resulting in lower CTR. Specifically, the CTR of 1060 aluminum with a lower modulus was reduced by an additional 0.62×10^{-5} m^2·K/W compared to SS304 steel (Fig. 3(f)). Liu *et al.*[50] demonstrated that applying pressure after surface wetting of PC-TIMs further reduces CTR, primarily because the pressure facilitates the expulsion of residual air at the interface. However, due to the fragility of microelectronic devices, the applied pressure cannot be increased indefinitely. There is a threshold for thermal conduction enhancement that aligns with the pressure tolerance of electronic assemblies. Zhao *et al.*[55] demonstrated through testing that for PC-TIM, this optimal pressure can be set at 0.3 MPa.

The actual contact area is significantly influenced by contact pressure and surface roughness. Increasing contact pressure and reducing surface roughness effectively enhances the actual contact area, thereby reducing thermal contact resistance. Considering the two possible forms of PC-TIM, namely, the shape-stable state without leakage and the two-phase state with minor surface liquefaction, the mechanism for increasing the surface contact area differs accordingly. In the former, the surface is filled through mechanical deformation of the PC-TIM, with the filling effect influenced by temperature, pressure, elastic modulus, and surface morphology. In the latter, the filling of the interface is achieved through a combination of the rheological flow of the liquefied phase and mechanical deformation, with "rheological filling" being the dominant process. Due to the rheological nature of the liquid phase, this filling effect is generally more effective than in the shape-stable state. Consequently, in this scenario, the impact of the thermal conductivity of the liquid-phase PC-TIM on the CTR must also be considered. Table 2 summarizes the relationship between the thermal resistance of PC-TIM and the actual contact area. PC-TIMs improve interfacial heat transfer efficiency through increased wettability and enhanced thermal conductivity resulting from phase transitions. Current research focuses primarily on enhancing thermal conductivity, improving encapsulation stability, and optimizing thermal cycling performance. In the future, the development of PC-TIMs will continue to aim at further improving thermal efficiency, enhancing material stability, and integrating intelligent functionalities.

Table 2. Models for geometry-induced thermal resistance.[56–58]

State of PC-TIM	Model	Application
Shape-stable state[56,57]	$R_c = \frac{A_r \Delta T}{Q}, A_r \propto \frac{P \cdot \sigma}{E^* \cdot \bar{r}}, \frac{1}{E^*} = \frac{1-\nu_1^2}{E_1} + \frac{1-\nu_2^2}{E_2},$	traditional TIM; leak-free PC-TIM
Two-phase state[58]	$R_{c1} + R_{c2} = \left(\frac{\sigma_1+\sigma_2}{2K_{TIM}}\right)\left(\frac{A_{nominal}}{A_{real}}\right),$	pure PC-TIM; PC-TIM with trace leak

Shape-stable state: Q is the total heat flux across the contact interface, and A_r is the real contact area; P is the total loading force; σ is the surface roughness (standard deviation); E^* is the equivalent modulus of elasticity; E_1, E_2 are the moduli of elasticity of the two contacting materials and ν_1, ν_2 are the Poisson's ratios. $\bar{r}$ is the mean radius of curvature of the micro-convex body.
Two-phase state: σ_1 and σ_2 are the surface roughness of the two contacting surfaces; K_{TIM} is liquid thermal conductivity; $A_{nominal}$ and A_{real} are the nominal areas and the actual microscopic area of contact, respectively.

2.3. Mismatch of thermal expansion behaviors

Different materials exhibit varying expansion behaviors when heated, and the coefficients of thermal expansion (CTEs) of heat sources, heat sinks, and TIMs are often not aligned. Semiconductor and metal materials typically have lower CTEs,[59,60] while PC-TIMs based on organic compounds or paraffin waxes tend to have higher CTEs.[61] Additionally, when PCM transitions from solid to liquid, significant volume changes occur.[62,63] This mismatch in thermal expansion can result in increased interfacial stress and the for-

mation of gaps, ultimately reducing heat transfer efficiency, as shown in Fig. 4. The most extensively studied aspect of thermal expansion in PC-TIMs involves encapsulated structures, which provide effective containment and minimize CTE mismatches. It is important to note that PCMs behave distinctly in solid and liquid states, making the definition and measurement of CTE challenging in both conditions. Therefore, research on thermal expansion typically approaches the issue indirectly. Additionally, unlike metal-based TIMs used in high heat flux applications, PC-TIMs are generally less sensitive to mechanical stress and are often encapsulated in microcapsules or specialized containers, which help mitigate the impact of volume changes during use.

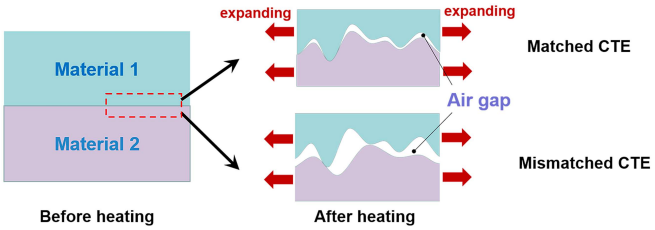


Fig. 4. Schematic representation of the effect of CTE matching at the interface on thermal resistance after exposure to heat.

2.4. Mechanisms and strategies for improving intrinsic thermal conductivity

The widely studied PC-TIMs are primarily categorized into organic PCMs and low-temperature liquid metals (LM) based on the specific application scenarios. Organic PCMs are typically composed of long-chain molecules and complex organic compounds. The weak van der Waals forces between molecules, coupled with a high degree of molecular disorder, significantly disrupt the conduction pathways for phonons, resulting in inherently low thermal conductivity (< 0.5 W/(m·K)).[64] Their low electrical conductivity makes them more suitable for applications requiring electrical insulation. The metallic nature of LM imparts high thermal and electrical conductivity, making it suitable for applications with high heat dissipation requirements where insulation is not essential.[65] Table 3 compares the performance parameters and characteristics of PC-TIM with commercial TIMs, along with their respective application scenarios. The following discussion on intrinsic thermal conductivity will focus on three aspects: theories, strategies, and predictive models.

Table 3. Key performance parameters of common TIM and PC-TIM.

	Type	K_{TIM}	R_{total}	Electrical conduction	Reusable
Commercial TIMs	grease	low	low	insulated	no
	pad	low	high	insulated	yes
	gel	low	high	insulated	no
	film	high	middle	tailored	no
PC-TIMs	organic-based	middle	low	insulated	yes
	LM-based	middle	middle	mostly conductive	yes

2.4.1. Thermal conduction mechanism

To ensure the reliability of PC-TIM, it is generally necessary to prepare PC-TIM as a composite system. Thermal conductivity theories provide insights for improving the thermal conductivity of composite material systems. Among them, the most widely accepted thermal conductivity theories include the thermal pathway theory, thermal percolation theory, and thermal elastic coefficient theory. The thermal pathway theory posits that when thermally conductive fillers are distributed in the polymer matrix to a certain volume fraction and form a continuous network, heat can be efficiently transferred through direct contact between fillers, significantly enhancing the thermal conductivity of the composite material (Fig. 5(a)).[66–68] This theory emphasizes the dominance of filler geometric arrangement and network connectivity in thermal conductivity performance. Its guiding principle for improving the thermal conductivity of composite materials is to add fillers exceeding the volume fraction threshold, adopt a network-chain spatial distribution configuration, and enhance the orientation of filler particles. The thermal percolation theory draws on the phenomenon of electrical percolation, indicating that when the filler volume fraction reaches the percolation threshold, a conductive network suddenly forms, causing a nonlinear leap in thermal conductivity (Fig. 5(b)).[69,70] This theory highlights the existence of a critical threshold and the synergistic effect of fillers on network connectivity. It is worth noting that there is indeed a certain correlation between the above two theories: Thermal percolation theory is typically grounded in the framework of statistical physics, emphasizing the formation of continuous conductive networks when the filler content in a composite exceeds a certain volume fraction, resulting in a significant enhancement of thermal conductivity and characterized by a well-defined percolation threshold. In contrast, the term thermal pathway is more descriptive, referring to the process of constructing continuous heat conduction routes among fillers. It highlights aspects such as the connectivity between fillers, interfacial thermal resistance, and the continuity and efficiency of the pathways. The thermal elastic coefficient theory, from the perspective of phonon transport, believes that the thermal conductivity of composite materials is determined by the degree of thermal elastic matching between fillers and the matrix (Fig. 5(c)).[71] Phonon scattering at the interface between the two phases is the main source of thermal resistance, and optimizing the thermal elastic matching at the interface can reduce scattering losses. Moreover,

the phonon transport mechanism, as another widely adopted approach, primarily addresses phonon-mediated heat conduction in non-metallic composite systems.[66] Interfacial phonon scattering (arising from factors such as mass mismatch or geometric misalignment) represents a primary contributor to interfacial thermal resistance. With ongoing research advancements and improved fabrication techniques, the design of composite materials is increasingly guided by filler orientation and the suppression of interfacial thermal resistance at the filler-matrix interface. This implies the necessity of incorporating the theoretical frameworks into a multiscale thermal conduction model to enable more accurate prediction and evaluation of thermal performance in composite systems.

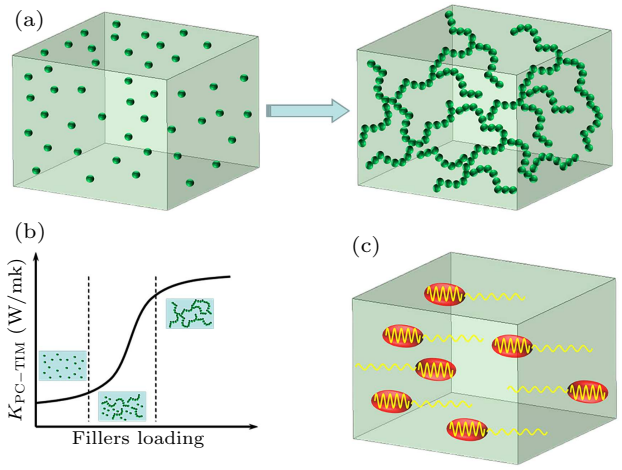


Fig. 5. Diagram of (a) thermal pathway theory; (b) thermal percolation theory; (c) thermal elastic coefficient theory.

2.4.2. Models for thermal conductivity

It is challenging to perform *in-situ* measurements of the thermal conductivity during the phase transition, and describing heat transfer using the pre-phase-change thermal conductivity is not entirely accurate.[72–74] This is because the thermal conductivity of PCMs is not constant during phase transitions. During this process, the molecular structure (in organic PCMs) or ionic bonds (in LMs) change, affecting the movement of heat carriers. Moreover, the accuracy of traditional thermal conductivity testing methods for PC-TIMs is significantly reduced. This is primarily due to two factors: (1) the material exhibits a heterogeneous phase of both liquid and solid states at temperatures close to the melting point; (2) the heat flux through the sample is significantly distorted due to the release and absorption of latent heat. The thermal conductivity of PCMs is typically estimated through numerical simulation.

The mathematical description of the phase boundary (Stefan boundary problem) during the phase change process, considering the heat transfer involved, enables the estimation of the thermal conductivity variation of the PCM during the phase transition.[75–77] Typically, the geometry of the PCM is approximated as regular shapes (such as cylinders or spheres), and by controlling the boundary conditions, the Stefan boundary problem can be simplified to a 1D transient heat transfer model.[78,79] However, for composite PC-TIMs, the phase change morphology of the PCM varies across different encapsulation strategies, complicating the calculation of thermal conductivity. In addition, within composite systems, the thermal conductivity of the material itself (including conductive fillers, PCM, and encapsulating matrix), the $R_{\text{filler/filler}}$ and the $R_{\text{filler/matrix}}$, as well as the effects of filler content, geometry, and topology should be considered. In this context, the effective medium approximation (EMA) model is a better choice.[80] However, the EMA model also has certain limitations: (1) it applies only to single-phase PC-TIMs; (2) it neglects the $R_{\text{filler/filler}}$, leading to potential calculation errors. Combining the Stefan boundary solution model with the EMA model holds promise for providing a solution to the calculation of thermal conductivity in the dynamic phase change process of PC-TIMs. Table 4 summarizes the calculation principles and applicability of the Stefan boundary solution model and the EMA model.

Table 4. The calculation principles and applicability of the Stefan boundary solution model and the EMA model.[79,81,82]

Method	Equation	Application
Stefan solution	cylindrical coordinate system:[81] $-K_{\text{l}}\left.\frac{\partial T_{\text{l}}}{\partial r}\right\|_{r=s(t)}+K_{\text{s}}\left.\frac{\partial T_{\text{s}}}{\partial r}\right\|_{r=s(t)}=\rho_{\text{s}}L\frac{\text{d}s(t)}{\text{d}t}$, $s(t)=2\lambda(\alpha_{\text{l}}t)^{1/2}$, spherical coordinate system:[79] $-Ste\left.\frac{\partial\overline{\theta}}{\partial\overline{r}}\right\|_{\overline{r}=\overline{x}}=\frac{\text{d}\overline{x}}{\text{d}\overline{\tau}}$, $Ste=\frac{c_{\text{p,l}}\cdot\Delta T}{L}$	pure PC-TIM with phase change considered
EMA[82]	$K_{\perp}=K_{\text{matrix}}\frac{1+f\left[\varepsilon_{\parallel}(1-J_{\parallel})(1-\langle\cos^2\theta\rangle)+\varepsilon_{\perp}(1-J_{\perp})\langle\cos^2\theta\rangle\right]}{1-f\left[\varepsilon_{\parallel}J_{\parallel}(1-\langle\cos^2\theta\rangle)+\varepsilon_{\perp}J_{\perp}\langle\cos^2\theta\rangle\right]}$, $K_{\parallel}=K_{\text{matrix}}\frac{2+f\left[\varepsilon_{\parallel}(1-J_{\parallel})(1+\langle\cos^2\theta\rangle)+\varepsilon_{\perp}(1-J_{\perp})(1-\langle\cos^2\theta\rangle)\right]}{2-f\left[\varepsilon_{\parallel}J_{\parallel}(1+\langle\cos^2\theta\rangle)+\varepsilon_{\perp}J_{\perp}(1-\langle\cos^2\theta\rangle)\right]}$,	composite PC-TIM without phase change considered

Stefan solution (cylindrical coordinates): the subscripts l and s represent the liquid- and solid-phase, respectively; T, K, t, r, and L denote the temperature, thermal conductivity, time, the radial coordinates, and latent heat, respectively; $s(t)$ is the position of the phase interface; λ is the dimensionless parameters calculated by the equation $\frac{q}{4\pi}\exp\left(-\lambda^2\right)+\frac{K_{\text{s}}(T_0-T_{\text{m}})}{E_1\left(\lambda^2\alpha_{\text{l}}/\alpha_{\text{s}}\right)}\exp\left(-\lambda^2\alpha_{\text{l}}/\alpha_{\text{s}}\right)=\lambda^2\alpha_{\text{l}}\rho_{\text{s}}L$, where the subscripts m and 0 represent the melting temperature and the initial temperature, respectively, α, ρ, and q denote the thermal diffusivity, density, and heat flux.
Stefan solution (spherical coordinates): the subscript l represents the liquid-phase; $\overline{\theta}$, $\overline{r}$, $\overline{x}$, and $\overline{\tau}$ are dimensionless parameters about temperature, radius, the location of phase change surface, and time, respectively; c_{p}, ΔT, and L denote the specific heat capacity, the temperature difference, and the latent heat of the material; Ste is the Stefan number.
EMA: the subscripts $\perp$ and $\parallel$ represent the cross- and in-plane, respectively; f and J are the fraction and the geometric factor of fillers; θ is the angle between the cross-plane direction of the PC-TIM and the axis of symmetry of the fillers; ε is a dimensionless parameter about thermal conductivity.

2.4.3. Strategies for enhancing thermal conductivity

For polymer-based TIMs, severe phonon scattering caused by factors such as molecular chain disorder, grain boundaries, and interfacial defects significantly limits thermal conductivity. Material design strategies for thermal conductivity improvement have mainly focused on enhancing phonon transport efficiency. Efficient heat transfer can be achieved either by enhancing the intrinsic phonon mean-free path of polymer chains through structural design or by introducing secondary phase fillers with intrinsically longer phonon mean-free paths.[7] Zhu *et al.*[83] synthesized polyethylene glycol (PEG)-based block copolymers through molecular engineering by reacting the –N=C=O groups in diisocyanate with the –OH groups in PEG (Fig. 6(a)). The alignment of the PEG chains resulted in extensive π–π stacking, which enhanced phonon transport thereby increasing the thermal conductivity from 0.25 W/(m·K) to 0.35 W/(m·K). Meanwhile, this copolymer can be directly thermally pressed to phase change films with properties such as machinability and flexibility towards thermal interface applications without requiring additional encapsulation, as shown in the illustration in Fig. 6(a). However, it is worth noting that research on tuning intrinsic molecular structures is relatively limited, primarily because the introduction of block structures or molecular rearrangements often restricts the mobility of the main chains and hinders the crystallization behavior, resulting in a significant reduction in phase change enthalpy. Introducing highly thermally conductive fillers is the mainstream method with research primarily focusing on the alignment of fillers and their interfacial contact with the matrix material.[84,85] Enhancing thermal conductivity is achieved by constructing continuous thermal pathways and reducing the resistance between fillers ($R_{\text{filler/filler}}$) and filler/matrix ($R_{\text{filler/matrix}}$). For organic PC-TIMs, continuous thermal pathways are typically established through the incorporation of structural frameworks, which also function as encapsulating matrices. Yang *et al.*[86] created a thermally conductive framework by impregnating paraffin into a graphite powder skeleton formed after the evaporation of ammonium bicarbonate (Fig. 6(b)). This design ensured both excellent thermal stability and leakage resistance (virtually no leakage after $>$ 100 cycles), resulting in a thermal conductivity of 19.27 W/(m·K), accompanied by faster thermal response. Jiang *et al.*[87] impregnated paraffin into a 3D porous skeleton composed of self-bonded graphite fiber monoliths, as shown in Fig. 6(c). The $R_{\text{filler/filler}}$ was reduced through *in-situ* carbonization of the skeleton. The final PC-TIMs exhibited in-plane and out-of-plane thermal conductivities of 36.49 W/(m·K) and 2.9 W/(m·K), respectively, achieving a 48.4 °C temperature reduction in LED chip applications compared to pure PCM installed.

In contrast to organic PCMs, LMs have a higher intrinsic thermal conductivity ($\sim$ 30 W/(m·K)), which generally enables them to meet the thermal conductivity requirements of TIM2. However, LMs can leak upon heating and melting, potentially contaminating the circuit board and even causing short circuits. To address this issue, researchers have encapsulated LMs within flexible matrices. These matrices typically have low thermal conductivity, making the overall thermal conductivity enhancement of the system a key research focus. Research on the use of LMs as PC-TIMs has progressed through two stages: increasing the LM content and using LM as a binder for filler particles. Increasing the LM content primarily involves improving the dispersion of liquid metals through ultrasound and shear forces. Krings *et al.*[88] achieved uniform dispersion of LM in PDMS elastomers using shear forces. At 50 vol% LM content, the thermal conductivity of the PC-TIM increased from 0.25 W/(m·K) to $\sim$ 1.7 W/(m·K). Considering the weight increase associated with high LM filler content, they incorporated hollow silica microspheres into the LM droplets, as shown in Fig. 6(d). At a 50% addition level, the thermal conductivity slightly decreased from 1.7 W/(m·K) to 1.35 W/(m·K). They also found that after applying a 400% tensile strain, the thermal conductivity of the PC-TIM along the stretching direction increased to 3.8 W/(m·K). This was attributed to the ability of liquid-phase thermal fillers to alter their shape under strain, thereby enhancing thermal conductivity, a property not exhibited by other rigid fillers. Using LM as a binder for filler particles primarily exploits its liquid nature at low temperatures to create soft connections with conventional rigid thermal particles. Inspired by the structure and function of bone joints, Xie *et al.*[89] developed a thixotropic slurry composed of Al_2O_3 and LM (Ga–In–Sn), which was mixed with PDMS to produce LM-based PC-TIMs, as shown in Fig. 6(e). The resulting materials achieved a thermal conductivity of 6.7 W/(m·K), with the R_{total} reduced to 14 mm^2·K/W, resulting in a 5 ° C temperature reduction in chip cooling applications compared to commercial thermal grease. Similarly, Jia *et al.*[90] used LM (Ga–In–Sn) as a sintering agent for BN sheets at room temperature and employed hot-pressing techniques to fabricate LM-based PC-TIMs. These materials exhibited in-plane and out-of-plane thermal conductivities of 82.2 W/(m·K) and 20.6 W/(m·K), respectively, achieving an 8.6 °C and 8.0 °C temperature reduction in LED chip and CPU applications. Another report involves filling self-supporting porous frameworks with LMs. For example, Chen *et al.*[91] filled a combination of Bi–Sn–In alloy and Ag particles into a copper foam, resulting in a thermal conductivity of 42.7 W/(m·K) and a similar temperature reduction in chip applications, as shown in Fig. 6(f). However, it is crucial to select an appropriate pore size since smaller pores may not hold enough PCM while larger pores could lead to leakage issues.

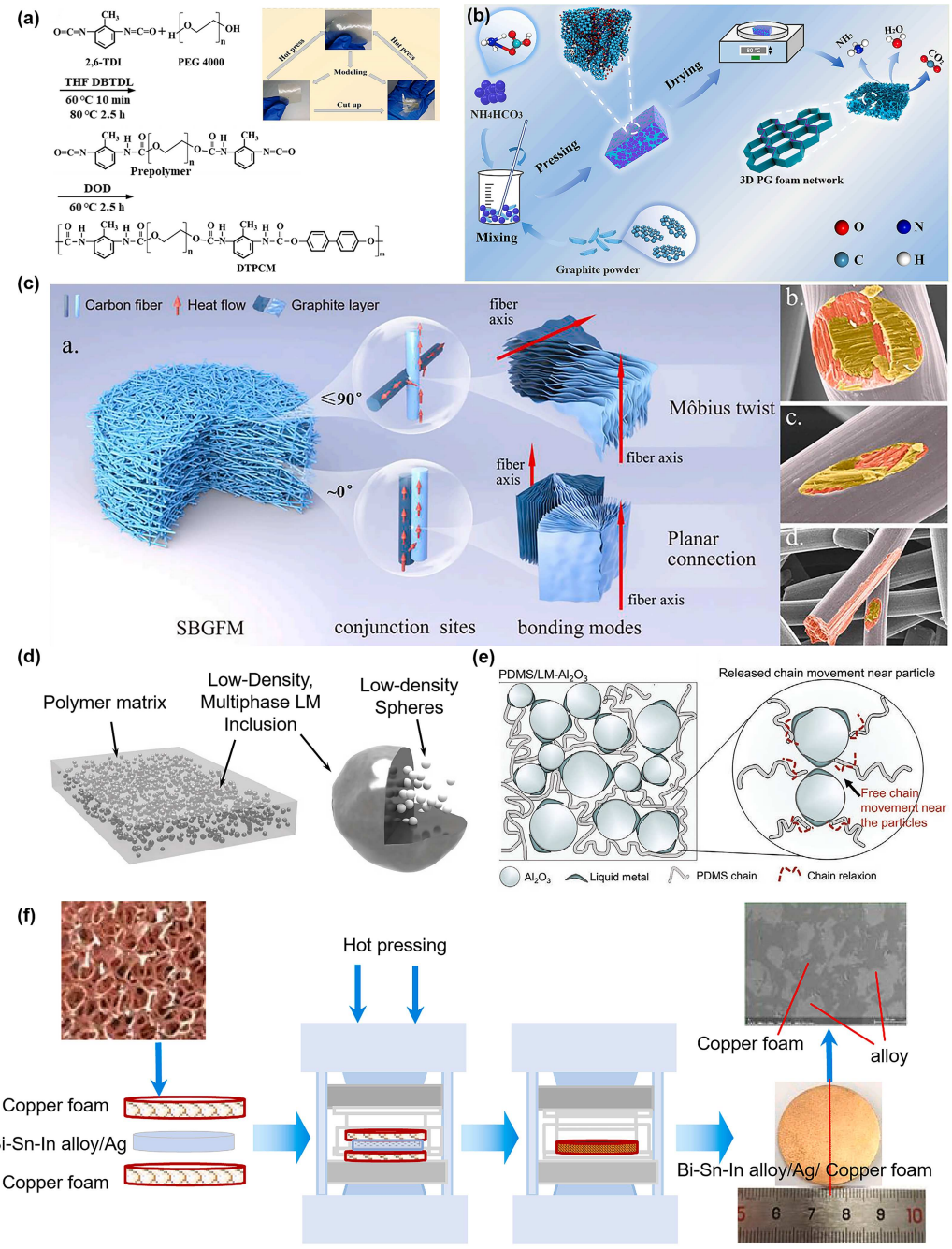


Fig. 6. (a) Reaction mechanism for the –N=C=O groups in diisocyanates with the –OH groups in PEG by Zhu *et al*, the inset shows the favorable flexibility, reproduced with permission from Ref. [83]; (b) preparation strategy of the thermally conductive framework composed of paraffin and graphite powder skeleton by Yang *et al*., reproduced with permission from Ref. [86]; (c) schematic of the 3D porous skeleton composed of self-bonded graphite fiber monoliths by Jiang *et al*., reproduced with permission from Ref. [87]; (d) material schematic showing the dispersion of multiphase LM inclusions embedded in a soft, elastomer matrix by Krings *et al*., reproduced with permission from Ref. [88]; (e) diagram of the internal structure of the prepared LM (Ga–In–Sn) based PC-TIM by Xie *et al*., reproduced with permission from Ref. [89]; (f) schematic illustration of the preparation process for present composites by Chen *et al*., reproduced with permission from Ref. [91].

The most effective strategy for enhancing the thermal conductivity of organic-based PC-TIMs remains the construction of conductive pathways within the composite system, with organic PCMs primarily functioning to wet the contact surfaces.[92] This has led to limited research on the intrinsic thermal conductivity of organic-based PC-TIMs. In contrast, for LM-based PC-TIMs, the primary role of LMs is to create soft connections with rigid thermal fillers, enhancing the formation of conductive pathways between the fillers and reducing the yield stress of the PC-TIM.

3. Encapsulation mechanisms and strategies

The primary purpose of encapsulation is to enhance the stability and lifetime of the material while mitigating the risks of leakage and chemical degradation during phase transitions.[93,94] The encapsulating structure not only provides mechanical support for PC-TIMs but also effectively

constrains morphological changes during phase transitions, thereby maintaining interface integrity and optimizing thermal conduction. The significance of encapsulation lies in its considerable impact on the overall performance of the material, ensuring stable and safe application in advanced electronic devices and high-efficiency energy conversion systems. Encapsulation strategies for PC-TIMs generally fall into three categories: physical adsorption via porous materials, the design of chain-crosslinked networks, and the formation of core–shell structures.

The porous materials, such as aerogels,[5] template-etched structures,[95] and open-cell foams,[96] can effectively immobilize PCMs within their pores through capillary action. To enhance thermal conductivity, porous materials with high-thermal-conductivity frameworks (such as expanded graphite[97] and metal foams[98]) are considered the most promising candidates. Dong *et al.*[99] prepared a PC-TIM by compressing paraffin adsorbed onto extended graphite (EG) through cold pressing (Fig. 7(a)), achieving significantly improved leakage resistance. The paraffin was retained within the EG framework by surface tension and capillary forces, resulting in minimal reductions in melting enthalpy and solidification enthalpy of 0.4% and 1.4% after 50 thermal cycles. Furthermore, the inherent high thermal conductivity of the EG increases the thermal conductivity of the PC-TIM to 24.887 W/(m·K), demonstrating superior thermal regulation (with surface temperatures during heating 5.2 °C higher than those of pure PCM). However, since EG usually exists in a powder form, its discontinuous macroscopic structure increases thermal resistance between adjacent particles and reduces the flexibility of the PC-TIM. Compared to carbon-based and inorganic porous frameworks, covalent organic frameworks (COFs) exhibit stronger interactions with PCMs, further enhancing leakage prevention. Luo *et al.*[100] incorporated COFs to improve the adsorption of PEG within reduced graphene oxide (rGO) aerogels, Fig. 7(b). This enhancement is attributed to the extensive hydrogen bonding formed between the C, N, and O atoms of the COF and PEG, resulting in a maximum encapsulation capacity of 96.1 wt%, which is 1.7 wt% higher than that of rGO aerogels alone. The PEG leakage rate remained below 0.1 wt%, and no change in enthalpy was observed after 100 thermal cycles. Additionally, the presence of rGO increased the thermal conductivity of the PC-TIM to 0.455 W/(m·K). It is noteworthy that parameters of porous frameworks, such as porosity,[101,102] pore geometry,[103] and skeleton thermal conductivity,[101] significantly influence PC-TIM performance, particularly in terms of phase-change behavior and thermal conductivity. High porosity coupled with high-thermal-conductivity skeletons can accelerate phase-change rates, while unique framework geometries may induce directional thermal conductivity. Additionally, the lower thermal resistance between the framework and PCM enhances overall thermal conductivity and accelerates PCM melting. However, porous frameworks may have weaker adsorption forces on PCMs, reducing the durability of PC-TIMs.[104] Moreover, high-viscosity PCMs may have difficulty penetrating the framework, leaving residual air pockets that impede heat transfer.[103,105] Overall, the porous framework adsorption strategy offers advantages in improving heat transfer and preventing leakage. By adjusting parameters such as porosity and pore size distribution, PC-TIMs can be tailored for various applications. Nevertheless, challenges remain, including increased thermal resistance due to insufficiently tight or uniform contact between the framework and PCM, higher manufacturing costs due to complex preparation processes, and potential issues with volume expansion.

Unlike the adsorption mechanism in porous structures, the chain cross-linking network design involves introducing PCMs into the matrix before polymerization.[106–108] Through chemical or physical interactions between molecular chains, the PCM becomes securely entangled and encapsulated within the matrix structure. Due to the relatively strong intermolecular forces, this method generally provides superior encapsulation performance. Additionally, PC-TIMs require a certain degree of flexibility at room temperature, making elastomers commonly used as matrix materials owing to their high mechanical strength and well-established production methods.[109] Typical materials include ethylene-vinyl acetate copolymer (EVAC),[110] silicone rubber (SR),[111] polydimethylsiloxane (PDMS),[112–114] olefin block copolymer (OBC),[50] propylene-based elastomer (POE),[115,116] and polyborosiloxane elastomer (PBSE).[117] Hu *et al.*[110] developed a PC-TIM using EVAC as the elastomer, EG as the thermal additive, and paraffin as the PCM, as shown in Fig. 7(c). The PC-TIM was fabricated via a lamination method, and the in-plane thermal conductivity could reach 7.01 W/(m·K). The temperature was reduced by 6.5 °C when applied to battery cooling of the cell phone. Another typical material is the gel-based elastomer, such as hydrogel,[118,119] organic gels,[120,121] ion gels,[122,123] which offers favorable surface adhesion, facilitating the installation and fixation of PC-TIMs while further reducing CTR. However, solvent evaporation from the hydrogel during use may cause device failure.[124] Therefore, Cao *et al.*[125] replaced water in the hydrogel with PEG, creating a solvent-free phase change gel that maintained latent heat stability after 100 thermal cycles (Fig. 7(d)). The unique phase change flexibility improved contact with rough surfaces, reducing the temperature of a copper mesh heat source by 14.8 °C compared to non-deformable TIMs. It is worth noting that the enhancement of thermal conductivity in chain cross-linked PC-TIMs is generally limited and often

lower than that achieved with porous material-based PC-TIMs. This limitation arises from the difficulty of orienting thermally conductive additives within the matrix, which hinders the formation of effective heat transfer pathways. Moreover, a high content of thermal conductive additives can degrade the flexibility of PC-TIMs, further impeding interfacial heat transfer.

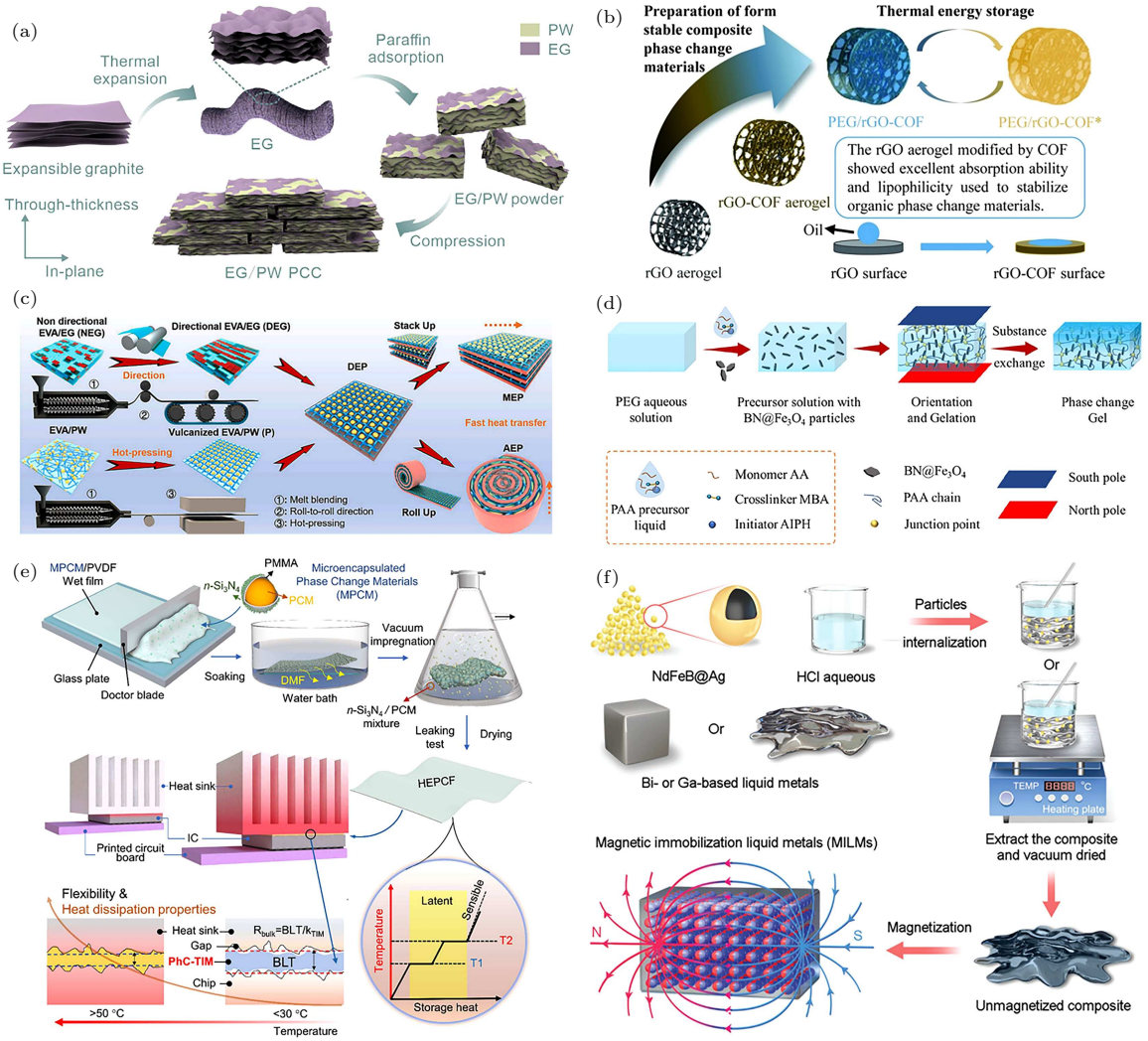


Fig. 7. (a) PC-TIM fabrication by compressing paraffin adsorbed onto EG through cold pressing by Dong *et al*., reproduced with permission from Ref. [99]; (b) incorporation of COFs for the PEG adsorption improvement within rGO aerogels by Luo *et al*., reproduced with permission from Ref. [100]. Schematic illustration of the preparation of PC-PCM using different elastomers as encapsulation matrix: (c) EVAC by Hu *et al*., reproduced with permission from Ref. [110]; (d) solvent-free phase change gel by Cao *et al*., reproduced with permission from Ref. [125]. Preparation strategies for PC-TIM with different core–shell structures: (e) phase change fibers by Lu *et al*., reproduced with permission from Ref. [130]; (f) thermally conductive magnetic particles as the oriented thermal conduction framework with LM as the PCM by Lu *et al*., reproduced with permission from Ref. [132].

In addition to the aforementioned two methods, the core–shell structure design is renowned for its optimal encapsulation performance. The term "core–shell structure" here generally refers to a configuration in which the PCM serves as the core, encapsulated by an organic or inorganic shell material.[61] This design isolates the PCM, confining phase transitions to a limited and enclosed space to achieve effective encapsulation.[126] The design of the shell thickness is critical: too thin shell could not sufficiently contain the PCM, while excessive thickness reduces the latent heat capacity. Core-shell structures are typically categorized into two types: phase-change microcapsules and phase-change fibers.[127–129] The former consists of PCM processed into discrete microbeads, whereas the latter encapsulates larger volumes of PCM into elongated fiber structures. To ensure the shell layer provides long-term stability in practical applications, core–shell structures often require additional processing (2nd encapsulation) to finalize the design, such as compression techniques or polymer chain locking. Lu *et al*.[130] prepared phase change fibers using coaxial electrospinning, with PEG as the core and thermoplastic polyurethane (TPU) as the shell, incorporating BNNS to improve thermal conductivity (Fig. 7(e)). The latent heat value remained at 96.3% even after 50 thermal cycles. In the thermal management of three types of chips in the 5G base station (main chips, timing chips, and RF chips), the PC-TIM outperformed commercial thermal silicone grease, achieving

temperature reductions of 11.5 °C, 4.5 °C, and 9.6 °C, respectively. Moreover, LMs exhibit the phenomenon of engulfing other metals, which provides a novel approach for reverse encapsulation.[88,131] Lu *et al.*[132] utilized silver-coated magnetic particles (NdFeB@Ag) as the core and leveraged the internal engulfing effect of liquid metal on the Ag layer to develop an innovative PC-TIM (Fig. 7(f)). No obvious leakage was observed even after three thermal cycles and mechanically induced deformations, owing to the strong interaction between the LM and the Ag layer, which effectively locked the LM phase in place. After 100 thermal cycles, the decrease in latent heat was only 2.07%. With a high thermal conductivity of 17.29 W/(m·K) and a low R_{total} value of 0.055 K·cm^2/W, this PC-TIM achieved a temperature reduction of 48 °C when applied to LED cooling. It is important to note that the 2nd encapsulation of core–shell structures may introduce additional interfacial layers, potentially increasing thermal resistance and reducing overall thermal efficiency. If the shell material lacks sufficient elasticity or deformability, it may lead to shell cracking or failure, compromising the encapsulation performance. Table 5 compares the characteristics of three encapsulation strategies in terms of leakage prevention, thermal conductivity enhancement, and flexibility.

Table 5. Comparison of the three encapsulation strategies.

Encapsulation strategy	Anti-leakage improvement	Thermal conductivity enhancement	Flexibility
Physical adsorption	limited (weak capillary force)	dramatic (high thermal conduction of the skeleton)	poor (depending on the flexibility of the skeleton)
Chain-crosslinked networks	obvious (strong chain interaction)	limited (incomplete heat conduction pathways)	favorable (provided by interaction structure)
Core–shell structure	dramatic (fully enclosed encapsulation)	obvious (high thermal conduction of the shell)	favorable (elastic housing for protection)

4. Extended applications

The application of PC-TIMs in electronic device cooling primarily focuses on their heat transfer and leakage prevention capabilities, with relatively few studies addressing the latent heat storage characteristics inherent to their phase change properties. This emphasis arises because the primary concern in electronic device cooling is the effective heat conduction to prevent overheating. In this context, the thermal conductivity and CTR of PC-TIMs become their most critical performance metrics, as the main task is to rapidly reduce temperature. Electronic devices often operate in high-frequency switching modes, where heat must be managed in real time. The latent heat storage feature is more effective during gradual temperature increases and is typically unable to respond quickly to rapid heat load fluctuations. However, the seamless integration of phase change behaviors and interfacial wetting properties endows PC-TIM materials with the capability to function as specialized TIMs across diverse application domains, including thermoelectric systems, thermochromic devices, thermosensor, and personal health management. This unique combination enables them to deliver high-performance thermal management solutions.

Thermoelectric devices contain pairs of P- and N-type semiconductors, functioning as thermoelectric coolers (TEC, Peltier effect) or generators (TEG, Seebeck effect).[133] TECs offer fast response and refrigerant-free operation. Integrating PC-TIMs with TECs (PC-TEC) improves temperature control duration and reduces power consumption. Efficient hot-side heat dissipation is critical to prevent efficiency loss from heat backflow.[134] Ren *et al.*[135] used BN, PEG, and PDMS as the top heat sink layer, Ni foam, BN, PEG, and PDMS as the intermediate PC-TIM layer, and TEC with PDMS as the bottom TEC layer to assemble a multilayer flexible PC-TEC. The heat sink layer together with the PC-TIM layer improved the cooling performance of the TEC by 55%. In the practical personal thermal management tests, a current supply of 0.45 A demonstrated better cooling performance than 0.7 A, achieving a temperature drop of 4.2 °C, as shown in Fig. 8(a). PC-TEG integration harnesses temperature differences to generate power, supplementing energy for smart electronics.[136,137] Sun *et al.*[138] incorporated graphene clusters into phase change microcapsules, observing an improved thermal conductivity (103 W/(m·K) at in-plane direction, 12 W/(m·K) at cross-plane direction) and a higher phase change enthalpy (94.2 J/g). When integrated with the TEG, the device achieved an open-circuit voltage of 1.6 V and an output power of 50 mW, which can power various electronic devices, as shown in Fig. 8(b). Future work will focus on optimizing thermoelectric-PCM thermal design, developing adaptive regulation, and integrating smart controls.

PCM heat exchange triggers temperature-driven color changes in thermochromic materials. This enables applications like smart windows, coatings, and sensors where visual temperature response is needed for indication or adaptive control.[139] Wang *et al.*[140] developed a smart wristband using paraffin/nonadecane/PDMS flexible phase change fibers with dual phase transition temperatures, combined with 6′-(diethylamino)-1′, 2′-benzofuran functioning as thermochromic agents, resulting in a color evolution across three stages. Their work demonstrates the potential for high-temperature warning and human thermal management applications (Fig. 8(c)). Current research focuses on aligning PCM thermal output with thermochromic thresholds.

Future work will develop hybrid systems combining PC-TIMs, thermochromics, and smart materials (e.g., self-healing/conductive) for next-generation wearables, health sensors, and adaptive construction.

Smart sensors enable real-time thermal management in PC-TIM systems. Their interconnectivity and monitoring capabilities allow dynamic temperature control.[141] Guo *et al*.[142] developed phase-change microspheres with high thermal conductivity and excellent stability based on paraffin/polydopamine/graphene blends. The electron–hole pairs in graphene dynamically balance with temperature changes, while the phase change of paraffin induces internal stress in the material, resulting in a change in electrical resistance. This property can be utilized in temperature sensing applications (Fig. 8(d)). Current PC-TIM/thermosensor integration faces challenges in achieving rapid heat transfer and response synchronization while mitigating phase-change-induced errors (e.g., thermal expansion/stress). Future research must focus on developing extremely durable sensors with improved accuracy while optimizing thermal response characteristics to enhance system compatibility and coupling performance.

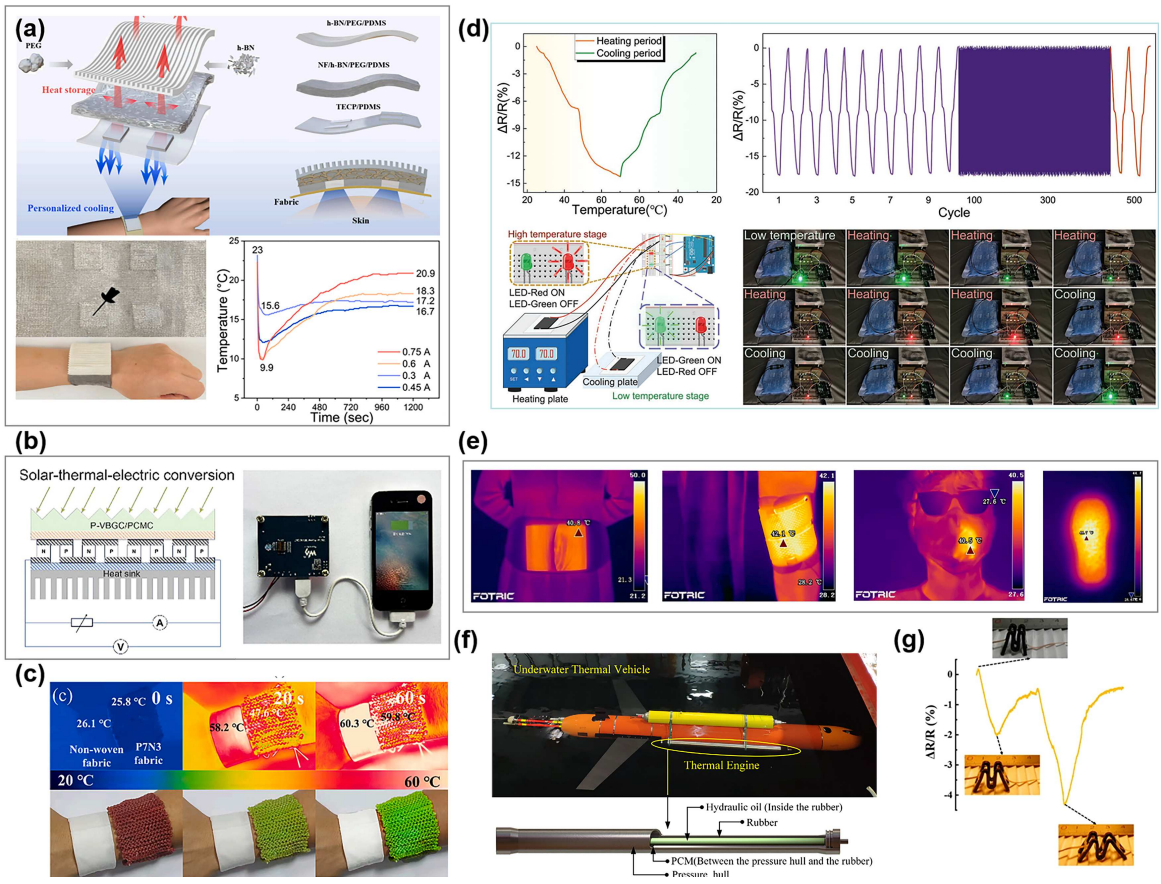


Fig. 8. (a) The preparation and performance tests of the multilayer flexible PC-TE by Ren *et al*., reproduced with permission from Ref. [135]; (b) PC-TEG driven by photothermal conversion by Sun *et al*., reproduced with permission from Ref. [138]; (c) temperature-regulating wristband with tricolor transition functionality designed by Wang *et al*., reproduced with permission from Ref. [140]; (d) phase change-driven temperature sensor by Guo *et al*., reproduced with permission from Ref. [142]; (e) the designed flexible PCMs used for thermal management devices (including a belt, knee protector, mask, and footpad) by Lin *et al*., reproduced with permission from Ref. [145]; (f) heat engine utilizing volume changes during phase transitions of PCMs by Wang *et al*., reproduced with permission from Ref. [146]; (g) robot driven by volume changes during phase transitions of PCMs by Xu *et al*., reproduced with permission from Ref. [147].

PCMs can serve as the interface layer between the skin and the external environment, making the thermal energy storage and release capabilities of PC-TIMs highly promising for personal thermal management applications.[143,144] Lin *et al*.[145] prepared flexible PCMs based on SEBS, EG, paraffin, and silicone oil, which offer a high energy storage density of 164.5 J/g, a large volume electrical conductivity of 193.76 S/cm, and a high thermal conductivity larger than 3.5 W/(m·K). The high electrical and thermal conductivities make it suitable as a core component for electric heating, with promising applications in thermal therapy for the human body, such as for the waist and joints (Fig. 8(e)). The key challenges persist in PC-TIM applications: slow dynamic response to rapid environmental/human activity changes, phase-change-induced uneven heating/expansion affecting comfort, and material biocompatibility concerns. Future development priorities include boosting thermal conductivity, improving response speeds, and enabling multifunctional integration for wearable/smart clothing applications.

The volume change induced by phase transitions in PCM

can drive thermal engines, making it a promising environmentally friendly power source. Wang *et al.*[146] discovered that the thermal conductivity of n-hexadecane gradually increases as it transitions from solid to liquid. Upon adding an appropriate amount of graphene, the thermal conductivity further improves. Based on these findings, they designed a thermal engine that reduced the energy storage time of the accumulator from 35.23 min to 31.01 min, meeting the power requirements of underwater vehicles (Fig. 8(f)). Another application field is biomimetic science, which involves mimicking the sensorymotor functions of biological neuromuscular systems, which requires materials with both sensing and driving capabilities. Xu *et al.*[147] demonstrated that internal stress generated by PCMs can induce reversible deformation, which could enable the contact and separation of conducting components (CNTs). This process effectively modulates the conductive network: when CNTs are in contact, the network is formed, and when CNTs are separated, the network is broken. Based on the electrical signal change, they developed a walking robot integrated with a feedback-controlled system (Fig. 8(g)). It can be summarized that the extended applications of PC-TIMs are primarily based on the secondary utilization of the thermal energy they store. Specific application scenarios include but are not limited to aerospace, underwater equipment, energy storage and conversion, and biomimetic science.

5. Conclusions and prospects

This paper provides a comprehensive review of PC-TIMs from three key perspectives: heat transfer enhancement, encapsulation strategies, and extended applications. The interface section considers factors affecting contact heat transfer, including the mismatch of thermal carriers at the microscale and contact geometry at the macroscale. The mechanisms influencing various physical properties and the optimization strategies are also systematically reviewed. For the heat transfer enhancement, the discussion focuses on intrinsic thermal conductivity improvements and interfacial heat transfer optimization. In terms of encapsulation strategies, three common methods are discussed: physical adsorption via porous materials, the design of chain-crosslinked networks, and the design of core–shell structures. The effects of each encapsulation strategy on leakage prevention, heat transfer enhancement, and flexibility are summarized. Finally, the manuscript explores the application of PC-TIMs in thermal energy storage, highlighting their coupling with thermoelectric, thermochromic, and thermosensing technologies for extended applications.

The emerging trends in PC-TIMs focus on the development of multifunctional composite materials, characterized by high thermal conductivity, self-healing capabilities, smart responsiveness, and broad applicability, as well as scalable industrial manufacturing processes. Standardization efforts and cross-scale modeling will further bridge laboratory innovations to high-reliability applications in 6G communications and quantum computing. While significant progress has been made in recent years, several challenges remain and they are presented below.

(1) There is a lack of comprehensive models for calculating the thermal conductivity of composite PC-TIMs. Existing models for thermal conductivity are limited in scope, typically applied to pure PCMs or simple composite materials, and do not align across scales. The underlying reason for this is the unclear impact of each component on heat transfer during the phase change process. The heat conduction mechanisms differ between the solid, liquid, and interface transition regions, significantly increasing the complexity and computational difficulty of thermal conductivity models. The future direction lies in the development of multiscale modeling approaches that consider the interactions, conduction, and interface effects of heat carriers from atomic to macroscopic scales. Additionally, the dynamic behavior of materials in the solid–liquid transition zone under thermal gradients should be considered, along with the development of time-varying thermal resistance models based on nonequilibrium heat conduction theory.

(2) The evaluation of the thermal performance of PC-TIMs is currently limited to basic material tests, such as thermal conductivity and CTR, with a lack of assessment methods for their performance during actual use. Electronic devices undergo complex thermodynamic and mechanical processes during operation, including heat generation, thermal expansion, mechanical stress, and increased thermal resistance. Currently, there is a lack of comprehensive evaluation and performance monitoring methods for PC-TIMs under long-term, high-power, and high-temperature gradient conditions. Further research is needed to develop coupled models for multiple physical fields, including thermal, mechanical, and electrical interactions, in combination with real-time monitoring techniques. This will enable dynamic evaluation of the thermal performance changes, stress distribution, and the impact on overall system performance during PC-TIM operation.

(3) Research on materials for enhancing the thermal conductivity of PC-TIMs and designing packaging frameworks is still in the exploratory stage. Traditional experimental methods for material screening are often time-consuming and costly, resulting in low efficiency in performance improvement. Machine learning algorithms (such as deep learning and support vector machines) can analyze large materials databases for prediction, thereby accelerating the discovery and design of PC-TIMs.[144] Additionally, machine learning algorithms (such as reinforcement learning and genetic algorithms) can be used to investigate the influence of material composition, arrangement, shape, and interface characteristics on heat transfer performance.[149,150] Given the diverse application scenarios and varying material performance

requirements, the future development of PC-TIMs must integrate data-driven AI approaches, enabling the maximization of benefits with minimal trial-and-error costs.

In summary, phase-change thermal interface materials are anticipated to evolve toward enhanced performance, multifunctionality, and sustainability, driven by advancements in materials science, engineering technologies, and growing application demands.

Acknowledgements

The authors acknowledge funding from the National Natural Science Foundation of China (Grant Nos. 52306214, 52425601, and 52276074), the Shanghai Chenguang Plan Program (Grant No. 22CGA78), and the National Key Research and the Development Program of China (Grant No. 2023YFB4404104).

References

[1] Li J, Zhou Y, Jiang C, Lei D and Yu X 2024 *J. Mater. Chem. C* **12** 12179
[2] Wang S, Zhao X, Luo J, Zhuang L and Zou D 2022 *Compos. Part A Appl. Sci. Manuf.* **163** 107216
[3] Zheng W, Shao C, Wang Q, Li G and Li H 2023 *Surf. Interfaces* **43** 103538
[4] Dai W, Wang Y, Li M, Chen L, Yan Q, Yu J, Jiang N and Lin C T 2024 *Adv. Mater.* **36** e2311335
[5] Hu B, Guo H, Li T, Li J, Cao M, Qi W, Li X and Li B 2024 *Chem. Eng. J.* **483** 149240
[6] Xing W, Xu Y, Song C and Deng T 2022 *Nanomaterials (Basel)* **12** 3365
[7] Zhao C, Li Y, Liu Y, Xie H and Yu W 2023 *Adv. Compos. Hybrid Mater.* **6** 27
[8] Wei B, Luo W, Du J, Ding Y, Guo Y, Zhu G, Zhu Y and Li B 2024 *SusMat* **4** e239
[9] Zhao X, Zou D and Wang S 2022 *Chem. Eng. J.* **431** 134231
[10] Liu C, Xu H, Yang J, Xie H and Yu W 2022 *Int. J. Therm. Sci.* **179** 107679
[11] Zhao X, Peng L M, Chen Y, Zha X J, Li W D, Bai L, Ke K, Bao R Y, Yang M B and Yang W 2021 *Mater. Horiz.* **8** 1230
[12] Khan J, Momin S A and Mariatti M 2020 *Carbon* **168** 65
[13] Lewis J S, Perrier T, Barani Z, Kargar F and Balandin A A 2021 *Nanotechnology* **32** 142003
[14] Ma H, Gao B, Wang M, Yuan Z, Shen J, Zhao J and Feng Y 2020 *J. Mater. Sci.* **56** 1064
[15] Feng C P, Yang L Y, Yang J, Bai L, Bao R Y, Liu Z Y, Yang M B, Lan H B and Yang W 2020 *Compos. Commun.* **22** 100528
[16] Chen S, Deng Z and Liu J 2021 *Nanotechnology* **32** 092001
[17] Razeeb K M, Dalton E, Cross G L W and Robinson A J 2017 *Int. Mater. Rev.* **63** 1
[18] Liu L, Su D, Tang Y and Fang G 2016 *Renewable Sustainable Energy Rev.* **62** 305
[19] Wu S, Yan T, Kuai Z and Pan W 2020 *Energy Storage Mater.* **25** 251
[20] Safari A, Saidur R, Sulaiman F A, Xu Y and Dong J 2017 *Renewable Sustainable Energy Rev.* **70** 905
[21] Lin Y, Alva G and Fang G 2018 *Energy* **165** 685
[22] Umair M M, Zhang Y, Iqbal K, Zhang S and Tang B 2019 *Appl. Energy* **235** 846
[23] Shamberger P J and Bruno N M 2020 *Appl. Energy* **258** 113955
[24] Zhang P, Yuan P, Jiang X, Zhai S, Zeng J, Xian Y, Qin H and Yang D 2017 *Small* **14** 1702769
[25] Hansson J, Nilsson T M J, Ye L and Liu J 2017 *Int. Mater. Rev.* **63** 22
[26] Kapitza P L 1941 *Phys. Rev.* **60** 354
[27] Chen J, Xu X, Zhou J and Li B 2022 *Rev. Mod. Phys.* **94** 025002
[28] Zhou T, Zhao Y and Rao Z 2022 *Int. J. Heat Mass Transfer* **189** 122701
[29] Lu J, Yuan K, Sun F, Zheng K, Zhang Z, Zhu J, Wang X, Zhang X, Zhuang Y, Ma Y, Cao X, Zhang J and Tang D 2019 *ACS Appl. Mater. Interfaces* **11** 42708
[30] Mu L, He J, Li Y, Ji T, Mehra N, Shi Y and Zhu J 2017 *J. Phys. Chem. C* **121** 14204
[31] Mu L, Li Y, Mehra N, Ji T and Zhu J 2017 *ACS Appl. Mater. Interfaces* **9** 12138
[32] Zhang R, Liu M Y, Liu W, Li Z M and He Z Z 2023 *Case Stud. Therm. Eng.* **43** 102801
[33] Aalilija A, Gandin C A and Hachem E 2021 *Int. J. Therm. Sci.* **166** 106817
[34] Wu Y J, Yagi T and Xu Y 2021 *Int. J. Heat Mass Transfer* **180** 121766
[35] Zhao Y, Zeng X, Ren L, Xia X, Zeng X and Zhou J 2021 *Mater. Chem. Front.* **5** 5617
[36] Li M, Shakoori M A, Wang R and Li H 2024 *Chin. Phys. Lett.* **41** 016302
[37] Wu M, Shi R, Qi R, Li Y, Feng T, Liu B, Yan J, Li X, Liu Z, Wang T, Wei T, Liu Z, Du J, Chen J and Gao P 2023 *Chin. Phys. Lett.* **40** 036801
[38] Yu J, Hanafusa H and Higashi S 2024 *Appl. Phys. Express* **17** 036502
[39] Wang W, Yang C, Xiong S and Wang X 2023 *Int. J. Heat Mass Transfer* **213** 124326
[40] Xu B, Hu S, Hung S W, Shao C, Chandra H, Chen F R, Kodama T and Shiomi J 2021 *Sci. Adv.* **7** eabf8197
[41] Fan H, Wang M, Han D, Zhang J, Zhang J and Wang X 2020 *J. Phys. Chem. C* **124** 16748
[42] Young D A and Maris H J 1989 *Phys. Rev. B* **40** 3685
[43] Nazarychev V M, Glova A D, Volgin I V, Larin S V, Lyulin A V, Lyulin S V and Gurtovenko A A 2021 *Int. J. Heat Mass Transfer* **165** 120639
[44] Barrat J L and Chiaruttini F 2003 *Mol. Phys.* **101** 1605
[45] Wang J S, Wang J and Zeng N 2006 *Phys. Rev. B* **74** 033408
[46] Hu B, Bao W, Chen G, Wang Z and Tang D 2023 *Comput. Mater. Sci.* **230** 112485
[47] He J, Tao L, Xian W, Arbaugh T and Li Y 2022 *Nanoscale* **14** 17681
[48] Song L, Zhang Y, Yang W, Tan J and Cheng L 2021 *Polymers (Basel)* **13** 3732
[49] Li R, Hussain K, Liao M E, Huynh K, Hoque M S B, Wyant S, Koh Y R, Xu Z, Wang Y, Luccioni D P, Cheng Z, Shi J, Lee E, Graham S, Henry A, Hopkins P E, Goorsky M S, Khan M A and Luo T 2024 *ACS Appl. Mater. Interfaces* **16** 8109
[50] Liu C, Yu W, Chen C, Xie H and Cao B 2020 *Int. J. Heat Mass Transfer* **163** 120393
[51] Liu C, Yu W, Fan J, Li Y, Chen J, Fu J, Peng G and Liu J 2024 *Appl. Therm. Eng.* **241** 122396
[52] Ren X J, Tang Q F, Zhang H, Zhang J R, Du M and Tao W Q 2023 *Case Stud. Therm. Eng.* **49** 103226
[53] Wang C, Lin Q, Pan Z, Hong J, Shao H and Mai Y 2023 *Int. Commun. Heat Mass Transfer* **149** 107131
[54] Feng B, Zhang Y H, Tu J, Fan L W and Yu Z T 2021 *Int. J. Heat Mass Transfer* **176** 121407
[55] Zhao J W, Zhao R, Huo Y K and Cheng W L 2019 *Int. J. Heat Mass Transfer* **140** 705
[56] Greenwood J A and Williamson J B P 1966 *Proc. Math. Phys. Eng. Sci.* **295** 300
[57] Persson B N J 2006 *Surf. Sci. Rep.* **61** 201
[58] Prasher R S 2001 *J. Heat Transfer* **123** 969
[59] Han X, Huang Y, Wang J, Zhang S, Ding Z and Li T 2021 *Compos. Commun.* **24** 100665
[60] Jia Y, Li K, Xue L, Huang L, Ren J and Zhang S 2017 *J. Eur. Ceram. Soc.* **37** 3255
[61] Xu M, Shi C, Li P, Guo X, Wang B and Zou D 2024 *Adv. Funct. Mater.* **34** 2409884
[62] Hu M, Wang D, Kokogiannakis G, Darkwa J, Li Y, Wang L, Xu Q and Su W 2024 *Chem. Eng. J.* **479** 147855
[63] Wang S, Zhao X, Wang Z, Zhang Y, Wang H and Zou D 2023 *J. Cleaner Prod.* **417** 138058
[64] Li X, Sheng M, Gong S, Wu H, Chen X, Lu X and Qu J 2022 *Chem. Eng. J.* **430** 132928
[65] Wang H, Chen S, Zhu X, Yuan B, Sun X, Zhang J, Yang X, Wei Y and Liu J 2022 *Matter* **5** 2054
[66] Xu X, Zhou J and Chen J 2019 *Adv. Funct. Mater.* **30** 1904704
[67] Zhao H Y, Yu M Y, Liu J, Li X, Min P and Yu Z Z 2022 *Nano-Micro Lett.* **14** 129
[68] Tauseef ur R, Ali H M, Janjua M M, Sajjad U and Yan W M 2019 *Int. J. Heat Mass Transfer* **135** 649

[69] Zhan H, Nie Y, Chen Y, Bell J M and Gu Y 2019 *Adv. Funct. Mater.* **30** 1903841
[70] Shin S, Wang Q, Luo J and Chen R 2019 *Adv. Funct. Mater.* **30** 1904815
[71] Wang Z, Wu Z, Weng L, Ge S, Jiang D, Huang M, Mulvihill D M, Chen Q, Guo Z, Jazzar A, He X, Zhang X and Xu B B 2023 *Adv. Funct. Mater.* **33** 2301549
[72] Meng D, Zhao K, Zhao W and Jiang G 2017 *J. Wuhan Univ. Technol.* **32** 1048
[73] Nabil M and Khodadadi J M 2013 *Int. J. Heat Mass Transfer* **67** 301
[74] Venkitaraj K P and Suresh S 2017 *Exp. Therm. Fluid Sci.* **88** 73
[75] Zhang Y, Jiang Y and Jiang Y 1999 *Meas. Sci. Technol.* **10** 201
[76] Yang X-H and Liu J 2018 *Int. J. Heat Mass Transfer* **127** 457
[77] Zhang Y, Zhang X, Xu X and Lu M 2020 *J. Energy Storage* **27** 101062
[78] Zhou T, Liu X, Li Y, Sun Z and Zhou J 2017 *Int. J. Heat Mass Transfer* **111** 631
[79] Ma A, Cai C, Peng S and Zhou T 2023 *Int. J. Therm. Sci.* **184** 107987
[80] Mao L K, Liu Q, Chen H and Cheng W L 2024 *Int. J. Heat Mass Transfer* **227** 125512
[81] Zhou T, Yuan J and Li M 2020 *Int. Commun. Heat Mass Transfer* **119** 104959
[82] Nan C W, Birringer R, Clarke D R and Gleiter H 1997 *J. Appl. Phys.* **81** 6692
[83] Zhu G, Zou M, Luo W, Huang Y, Chen W, Hu X, Jiang X and Li Q 2024 *Chem. Eng. J.* **488** 150930
[84] Su M, Han G, Gao J, Feng Y, He C, Ma J, Liu C and Shen C 2022 *Chem. Eng. J.* **427** 131665
[85] Afaynou I, Faraji H, Choukairy K, Arshad A and ArıcıM 2023 *Int. Commun. Heat Mass Transfer* **143** 106690
[86] Yang X, Li C, Ma Y, Chi H, Hu Z and Xie J 2023 *Chem. Eng. J.* **473** 145364
[87] Jiang Z, Ouyang T, Ding L, Li W, Li W and Balogun M S 2022 *Chem. Eng. J.* **438** 135496
[88] Krings E J, Zhang H, Sarin S, Shield J E, Ryu S and Markvicka E J 2021 *Small* **17** e2104762
[89] Xie Z, Dou Z, Wu D, Zeng X, Feng Y, Tian Y, Fu Q and Wu K 2023 *Adv. Funct. Mater.* **33** 2214071
[90] Jia L C, Wang Z X, Wang L, Zeng J F, Du P Y, Yue Y F, Zhao L H and Jia S L 2023 *Mater. Horiz.* **10** 5656
[91] Chen K, Ding J, Wang W and Lu J 2023 *Chem. Eng. J.* **454** 140087
[92] Liu Y, Zheng R and Li J 2022 *Renewable Sustainable Energy Rev.* **168** 112783
[93] Huang Z J, Liu Y L, Zhu T Y, Jiang W J, Sun D X, Yang J H, Qi X D and Wang Y 2024 *J. Energy Storage* **98** 113043
[94] Zhang Z, Liu Y, Yang K, Chen D, Li S and Li Z 2022 *Mater. Chem. Phys.* **290** 126564
[95] Guo P, Sheng N, Zhu R, Zhu C and Rao Z 2023 *ACS Sustainable Chem. Eng.* **11** 3324
[96] Ki S, Shin S, Cho S, Bang S, Choi D and Nam Y 2024 *Adv. Sci.* **11** 2310185
[97] Jesus D'Oliveira E, Azimov U, Costa Pereira S C and Lafdi K 2024 *J. Energy Storage* **92** 112090
[98] Cui W, Si T, Li X, Li X, Lu L, Ma T and Wang Q 2022 *Renewable Sustainable Energy Rev.* **169** 112912
[99] Dong Q, Sun B, Dong Z, Tian Y, Zhu H, Yuan G, Cong Y, Li B, Guo J and Li X 2022 *Energy Rep.* **8** 7071
[100] Luo W, Zou M, Luo L, Chen W, Hu X, Ma Y, Li Q and Jiang X 2022 *ACS Appl. Mater. Interfaces* **14** 55098
[101] Yang Q, Yao H, Yang Y and Azaiez M 2024 *Energy* **300** 131532
[102] Huang X, Sun C, Chen Z and Han Y 2021 *Int. J. Therm. Sci.* **170** 107151
[103] Cai W, Yang W, Jiang Z, He F, Zhang K, He R, Wu J and Fan J 2019 *Sol. Energy Mater. Sol. Cells* **194** 111
[104] Zhang X, Su G, Lin J, Liu A, Wang C and Zhuang Y 2021 *Int. J. Heat Mass Transfer* **170** 121021
[105] Hamidi E, Ganesan P B, Sharma R K and Yong K W 2023 *Renewable Sustainable Energy Rev.* **176** 113196
[106] Qi S and Yuan W 2023 *Chem. Eng. J.* **473** 145329
[107] Yang L Y, Feng C P, Bai L, Bao R Y, Liu Z Y, Yang M B and Yang W 2021 *Chem. Eng. J.* **425** 131466
[108] Xu S, Cai S and Liu Z 2018 *ACS Appl. Mater. Interfaces* **10** 36352
[109] He Q, Qin M, Zhang H, Yue J, Peng L, Liu G, Feng Y and Feng W 2024 *Mater. Horiz.* **11** 531
[110] Hu X, Huang X, Quan B, Zhu C, Yang Y, Sheng M, Ding C, Wen H, Li X, Wei J, Wu H, Lu X and Qu J 2023 *Chem. Eng. J.* **471** 144720
[111] Zhao Y, Zhang Z, Cai C, Zhou Z, Ling Z and Fang X 2023 *Appl. Therm. Eng.* **230** 120807
[112] Zhou Y, Li S, Zhao Y, Ling Z, Zhang Z and Fang X 2022 *Compos. Sci. Technol.* **218** 109192
[113] Wei S, Wang W, Zhou L and Guo J 2022 *Compos. Part A Appl. Sci. Manuf.* **162** 107149
[114] Jiang W J, Wang R Q, Zhu T Y, Feng M, Sun D X, Yang J H, Qi X D and Wang Y 2024 *Chem. Eng. J.* **479** 147622
[115] Wei F, Feng C P, Yang J, Yang L Y, Bai L, Bao R Y, Liu Z Y, Yang M B and Yang W 2021 *ACS Appl. Mater. Interfaces* **13** 59364
[116] Kang L, Niu H, Ren L, Lv R, Guo H and Bai S 2023 *Chem. Eng. J.* **463** 142402
[117] Zhao C, Wang Y, Gao L, Xu Y, Fan Z, Liu X, Ni Y, Xuan S, Deng H and Gong X 2022 *ACS Appl. Mater. Interfaces* **14** 21564
[118] Hu Y, Zhuo H, Zhang Y, Lai H, Yi J, Chen Z, Peng X, Wang X, Liu C, Sun R and Zhong L 2021 *Adv. Funct. Mater.* **31** 2106761
[119] Yang J, Yu W, Liu C, Xie H and Xu H 2022 *Compos. Sci. Technol.* **219** 109223
[120] Kuzina M A, Kartsev D D, Stratonovich A V and Levkin P A 2023 *Adv. Funct. Mater.* **33** 2301421
[121] Zou L, Luo Y, Zhang J, Sheng X, Chen Y and Lin P 2023 *J. Energy Storage* **60** 106590
[122] Yan K, He B, Wu S, Zeng Y, Wang P, Liu S, Ye Q, Zhou F and Liu W 2024 *ACS Appl. Mater. Interfaces* **16** 30453
[123] Liu C, Yang J, Li Y, Fu J, Yu W and Xie H 2024 *Surf. Interfaces* **47** 104204
[124] Cheng P, Tang Z, Chen X, Xu J, Liu P, Zhang X and Wang G 2023 *Nano Energy* **105** 108009
[125] Cao H, Li Y, Xu W, Yang J, Liu Z, Bai L, Yang W and Yang M 2022 *ACS Appl. Mater. Interfaces* **14** 52411
[126] Do J Y, Son N, Shin J, Chava R K, Joo S W and Kang M 2021 *Mater. Des.* **198** 109357
[127] Guan J, Fan W, Li H, Mai Z, Jing Y, Chen J, Zhang M, Tang B, Yang Y and Shen X 2024 *Colloids Surf., A* **690** 133809
[128] Niu Z, Qi S, Shuaib S S A and Yuan W 2022 *Compos. Part B Eng.* **228** 109431
[129] Lin Y, Kang Q, Liu Y, Zhu Y, Jiang P, Mai Y W and Huang X 2023 *Nanomicro Lett.* **15** 31
[130] Lu Q, Wang X, Zhao H W, Wang X R, Zhao J Q, Kong H R, Wang T, Liang C, Li J H and Xu W Q 2022 *J. Mater. Chem. A* **10** 23617
[131] Wang M and Lin Y 2024 *Nanoscale* **16** 6915
[132] Lu Y, Yu D, Dong H, Chen S, Zhou H, Wang L, Deng Z, He Z and Liu J 2022 *Adv. Funct. Mater.* **33** 2210961
[133] Cai Y, Hong B H, Wu W X, Wang W W and Zhao F Y 2022 *Energy* **254** 124356
[134] Krishna V N, Manikandan S and Selvam C 2022 *Appl. Therm. Eng.* **212** 118612
[135] Ren S, Zhang M, Ye S, Wu K, Sun Z, Du Y and Fang J 2024 *Chem. Eng. J.* **499** 155914
[136] Malakooti M H, Kazem N, Yan J, Pan C, Markvicka E J, Matyjaszewski K and Majidi C 2019 *Adv. Funct. Mater.* **29** 1906098
[137] Huo W, Xia Z, Gao Y, Guo R and Huang X 2023 *ACS Appl. Mater. Interfaces* **15** 29330
[138] Sun L, Wang Y, Chen L, Ying J, Li Q, Fu L, Yan Q, Wu K, Xue C, Yu J, Jiang N, Nishimura K, Lin C T and Dai W 2024 *Mater. Horiz.* **11** 5031
[139] Crosby P H N and Netravali A N 2022 *Adv. Sustainable Syst.* **6** 2200208
[140] Wang R Q, He Y J, Xiao Y Y, Sun D X, Yang J H, Qi X D and Wang Y 2023 *Eur. Polym. J.* **187** 111890
[141] Yusuf A, Sánchez del Río J, Ao X, Olaizola I A and Wang D Y 2022 *Nano Energy* **103** 107790
[142] Guo H, Jiao W, Jin H, Yuan Z and He X 2022 *Adv. Funct. Mater.* **33** 2209345
[143] Luo T, Kong L, Li L, Lu J, Yu Z, Lin B, Fu L and Xu C 2024 *Chem. Eng. J.* **486** 150443
[144] Peng Y and Cui Y 2024 *Natl. Sci. Rev.* **11** nwae295
[145] Lin X, Ling Z, Fang X and Zhang Z 2022 *Appl. Energy* **327** 120141
[146] Wang G, Yang Y and Wang S 2022 *J. Mol. Liq.* **348** 118048
[147] Xu Z, Wei D W, Bao R Y, Wang Y, Ke K, Yang M B and Yang W 2022 *ACS Appl. Mater. Interfaces* **14** 22521
[148] Bhatasana M and Marconnet A 2021 *Appl. Therm. Eng.* **199** 117384
[149] Baeuerle S, Gebhardt M, Barth J, Mikut R and Steimer A 2024 *IEEE Access* **12** 17782
[150] Suh Y, Chandramowlishwaran A and Won Y 2024 *npj Computational Materials* **10** 65